Continuous mode cooling and phonon routers for phononic quantum networks

Continuous mode cooling and phonon routers for phononic quantum networks

2012 New J. Phys. 14 115004

(http://iopscience.iop.org/1367-2630/14/11/115004)

New Journal of Physics
The open-access journal for physics

Continuous mode cooling and phonon routers for phononic quantum networks

S J M Habraken[1,2,4], K Stannigel[1,2], M D Lukin[3], P Zoller[1,2] and P Rabl[1]

[1] Institute for Quantum Optics and Quantum Information of the Austrian Academy of Sciences, Innsbruck, Austria
[2] Institute for Theoretical Physics, University of Innsbruck, Austria
[3] Department of Physics, Harvard University, Cambridge, MA, USA
E-mail: steven.habraken@uibk.ac.at

New Journal of Physics **14** (2012) 115004 (32pp)
Received 27 May 2012
Published 5 November 2012
Online at http://www.njp.org/
doi:10.1088/1367-2630/14/11/115004

Abstract. We study the implementation of quantum state transfer protocols in phonon networks, where, in analogy to optical networks, quantum information is transmitted through propagating phonons in extended mechanical resonator arrays or phonon waveguides. We describe how the problem of a non-vanishing thermal occupation of the phononic quantum channel can be overcome by implementing optomechanical multi- and continuous mode cooling schemes to create a 'cold' frequency window for transmitting quantum states. In addition, we discuss the implementation of phonon circulators and switchable phonon routers, which rely only on strong coherent optomechanical interactions and do not require strong magnetic fields or specific materials. Both techniques can be applied and adapted to various physical implementations, where phonons coupled to spin- or charge-based qubits are used for on-chip networking applications.

[4] Author to whom any correspondence should be addressed.

Contents

1. Introduction

The successful application of laser cooling techniques to cooling isolated vibrational modes of micro- and nanomechanical devices [1–8] has recently led to much interest in the control of macroscopic phononic degrees of freedom at a single quantum level. By now, preparation of mechanical resonators close to their quantum ground state has been achieved in different experimental settings [9–11], and coherent interfaces between mechanics and other quantum systems such as superconducting qubits [9, 12], spins [13, 14] or photons [15, 16] are currently being developed. Besides offering new possibilities to address fundamental questions of quantum physics [17–20], these experimental developments also provide the foundation for new, phonon-based quantum technologies. For example, in the context of quantum information processing and quantum communication, optomechanical (OM) slowing of light [21, 22] and the first steps towards realizing a mechanical quantum memory [15, 16] have been demonstrated, and the use of mechanical quantum transducers for interfacing different qubit systems [23–25]

has been proposed. For these applications, mechanical systems benefit from the ability to interact with a wide range of other electric, magnetic and optical quantum systems, while still maintaining long coherence times and being compatible with scalable nano-fabrication techniques.

The use of phonons for quantum information science applications is not new. In the first proposals for quantum computers, it has already been suggested to employ vibrational modes of a trapped ion Wigner crystal for transmitting quantum information between spatially separated qubits [26]. More recently, it has been shown that these ideas could equally well be applied to systems of coupled macroscopic mechanical resonators [23, 27, 28], which extends the concept of a mechanical quantum bus to a wider range of atomic and solid-state systems. In analogy to optical fields, phonons can be confined in phonon cavities (e.g. represented by a high-Q mechanical resonator), but also propagate freely along phononic waveguides. This suggests that many quantum communication and state-transfer protocols developed in the context of optical quantum networks [29–31] could—on a smaller physical scale—also be implemented using acoustic phonons. Here, new approaches to design and pattern phonon waveguides based on phononic crystals structures [32, 33] provide a very promising and versatile platform for realizing such phonon networks in practice. However, compared with the relatively advanced field of optical quantum networks [30], many equivalent control techniques still have to be developed for phononic quantum systems, which face the additional challenge that thermal noise in phononic channels is not negligible and would usually by far exceed quantum signals encoded in a single phononic excitation.

In this paper, we address the problem of implementing quantum communication protocols in thermal phononic channels and show how the addition of OM control elements can be used to realize a faithful transfer of quantum information between different nodes of the network. As a first key element to achieve this task, we describe the generalization of OM laser cooling techniques to multi- and continuous mode setups. This approach is motivated by a recent proposal for interfacing OM systems (OMS) with phonon waveguides [25], and leads to a strong suppression of thermal noise within the relevant transmission bandwidth. Therefore, instead of pursuing the otherwise challenging task of cooling the whole network, this technique creates a ‘cold’ frequency window, which is sufficient to coherently transfer single quanta through an otherwise ‘hot’ phononic channel.

As a second control tool we describe the implementation of phonon circulators and switchable phonon routers, which enable a directed transfer of propagating phonons through large one-dimensional (1D) or 2D networks. In the optical domain, circulators or other non-reciprocal devices are usually based on the Faraday effect. In principle, similar effects also exist for acoustic phonons in certain materials [34]. However, due to the required large magnetic fields and the use of materials with non-optimized mechanical properties, this approach is not suited for on-chip phonon quantum networks. Instead, we propose an integrated circulator for acoustic phonons that relies solely on an OM-induced non-reciprocity [35, 36], where the directionality is imposed by the phase relation between two optical driving fields. Thereby, the device can be switched on or reversed conveniently and in combination with the above-mentioned cooling techniques, this coherent OM routing scheme is, in principle, sufficient to fully control the distribution of quantum information in large-scale phonon networks.

The remainder of this paper is structured as follows. In section 2, we first present a brief introduction to phonon networks and the general input–output formalism, which is used to

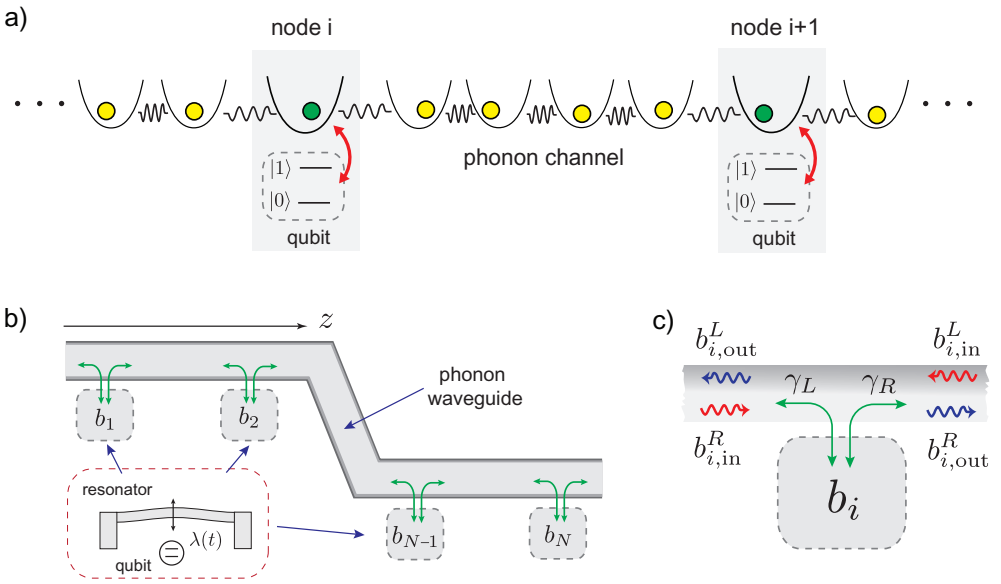

Figure 1. (a) Schematic representation of a generic phonon quantum network. At each node, qubits interact with a localized phonon mode, which in turn is weakly coupled to a phononic channel represented by an extended array of coupled mechanical resonators or a 1D phonon waveguide. (b) A phonon quantum network consisting of a set of localized vibrational modes, which are side coupled to a common phonon waveguide and mediate the interaction between qubits and the propagating phonon modes (for a specific implementation of such a setup, see [25]). (c) The localized phonons decay into left- and right-propagating modes in the waveguide with the corresponding rates γ_{L} and γ_{R}. The $b_{i,\mathrm{in}}^{\mathrm{L/R}}$ and $b_{i,\mathrm{out}}^{\mathrm{L/R}}$ denote the incident and outgoing waveguide fields at each node. See the main text for more details.

model these systems. In section 3, we revisit OM laser cooling and generalize it to multi- and continuous mode scenarios. As a basic application we then discuss in section 4 how an OM noise filter can be applied to transmit a quantum state through a thermal channel. In section 5, we describe the realization of phonon circulators and routers using coherent OM interactions. Finally, in section 6 we outline several potential systems for implementing phonon networks and then summarize the main results and conclusions in section 7.

2. Phonon quantum networks

Figure 1(a) shows a schematic representation of a generic phonon quantum network, where individual nodes $i = 1, \ldots, N$ are connected via a mechanical quantum bus. In analogy to optical quantum networks, each node contains an isolated solid-state two-level system ('qubit') with quantum information encoded in states $|0\rangle$ and $|1\rangle$. The qubits interact with localized phonon modes ('phonon cavities'), which are in turn weakly coupled to a common set of propagating modes of a phonon waveguide or a coupled mechanical resonator array ('quantum

channel'). The full Hamiltonian of this system is given by

$$H = \sum_{i=1}^{N} H^i_{\rm node} + H_{\rm channel} + H_{\rm int}, \tag{1}$$

where $H^i_{\rm node}$ and $H_{\rm channel}$ describe the dynamics of the individual nodes and the phononic channel, respectively, and $H_{\rm int}$ accounts for the coupling between them. In the following, we assume that the Hamiltonian for the individual nodes takes the form ($\hbar = 1$)

$$H^i_{\rm node}(t) = \omega_{\rm m} b_i^\dagger b_i + \frac{\Delta^i_{\rm q}(t)}{2}\sigma^i_z + \lambda_i(t)\left(\sigma^i_+ b_i + \sigma^i_- b_i^\dagger\right), \tag{2}$$

where σ^i_k are the Pauli operators and b_i the bosonic operators for the local mechanical modes of frequency $\omega_{\rm m}$. The third term describes the coupling between the qubits and the local mechanical modes. For each node the qubit frequency splitting $\Delta^i_{\rm q}(t)$ and the qubit–resonator coupling $\lambda_i(t)$ can be tuned independently by changing the qubit frequency or modulating the coupling with local control fields (see section 6). For $\omega_{\rm m} \sim \Delta^i_{\rm q}$ this allows for a controlled mapping of the qubit state onto a phonon superposition, which we will use in our discussion of the state transfer below. The implementation of qubit–resonator interactions as given in equation (2) has been described for various charge- and spin-based qubits in the literature and in section 6 we briefly summarize some of the most relevant systems.

2.1. Phonon channels

The mechanical quantum channel which is used to communicate between the nodes can, in general, be represented by a chain of $N_{\rm ch}$ coupled mechanical resonators,

$$H_{\rm channel} = \sum_{\ell=1}^{N_{\rm ch}} \frac{p_\ell^2}{2m} + \frac{1}{2}m\omega_0^2 x_\ell^2 + \frac{k}{2}\sum_{\ell=1}^{N_{\rm ch}-1}(x_\ell - x_{\ell+1})^2. \tag{3}$$

Here x_ℓ and p_ℓ are the position and momentum operators, m is the effective mass, ω_0 is the bare oscillation frequency and the spring constant k accounts for the nearest-neighbor coupling. For small $N_{\rm ch}$ the coupled resonators form a discrete set of collective eigenmodes. In this case quantum state transfer and quantum information processing protocols between two qubits can be implemented by addressing only a single collective mode, as has been discussed in the context of trapped ion systems [26] or coupled nanomechanical [23] and OM [28] resonators.

In this paper, we are primarily interested in the opposite regime of extended arrays, $N_{\rm ch} \gg 1$. In this limit $H_{\rm channel}$ can be represented by a dense set of plane wave modes, $H_{\rm channel} = \sum_q \omega_q b_q^\dagger b_q$, where $[b_q, b_{q'}^\dagger] = \delta_{q,q'}$, ω_q is the phonon dispersion relation, and for a lattice spacing a, the momentum label q is restricted to the first Brillouin zone $q \in (-\frac{\pi}{a}, \frac{\pi}{a}]$. This scenario is realized, for example, in large arrays of coupled nanomechanical beams [37] or in phononic band gap structures [32], where each resonator ℓ corresponds to a vibrational mode of a unit cell, typically of size $a \sim 1\,\mu$m. In the continuum limit we can identify a frequency range $\Delta\omega$ away from the band edges in which the coupled resonator array exhibits an approximately linear dispersion $\omega_q \approx \tilde{\omega}_0 + c|q|$, where c is the effective speed of sound and $\tilde{\omega}_0$ a frequency offset. In this case it is convenient to introduce the normalized displacement field $\Phi(z) = \Phi_{\rm R}(z) + \Phi_{\rm L}(z)$, where

$$\Phi_{\rm R}(z) = \sqrt{\frac{2c}{L}}\sum_{q>0} {\rm e}^{{\rm i}qz} b_q, \quad \Phi_{\rm L}(z) = \sqrt{\frac{2c}{L}}\sum_{q>0} {\rm e}^{-{\rm i}qz} b_{-q}, \tag{4}$$

describe right- and left-moving mechanical excitations of the phononic channel. Under the assumption of a linear dispersion these fields obey $[\Phi_{\mathrm{R}}(z,t), \Phi_{\mathrm{L}}^{\dagger}(z',t')] = 0$ and

$$[\Phi_{\mathrm{R/L}}(z,t), \Phi_{\mathrm{R/L}}^{\dagger}(z',t')] \simeq \mathrm{e}^{-\mathrm{i}\tilde{\omega}_0(t-t')}\delta(t-t' \mp (z-z')/c). \tag{5}$$

By assuming that the frequency of the local mechanical modes ω_{m} also lies within this frequency range, the coupling between the local resonators and the waveguide modes can be approximated by

$$H_{\mathrm{int}} \simeq \sqrt{\frac{\gamma}{2}} \int_0^L \mathrm{d}z \sum_{i=1}^{N} \delta(z-z_i)\left(b_i^{\dagger}\Phi(z) + b_i\Phi^{\dagger}(z)\right), \tag{6}$$

where L is the length of the waveguide and z_i are the positions of the nodes along the waveguide (see figure 1(b)). Below we identify γ as the total decay rate of the local resonator modes into the waveguide. Note that equations (5) and (6) are valid for times $|t-t'| > \Delta\omega^{-1}$ and distances $|z-z'| > a$. An explicit and more detailed derivation of these results is given in appendix A for the case of a simple coupled resonator chain.

2.2. *Input–output relations*

Under the validity of equations (5) and (6) and in the limit where ω_{m} and the bandwidth $\Delta\omega$ are large compared to the other characteristic frequency scales, we can eliminate the waveguide modes and use an input–output formalism [38] to describe the effective dynamics of the coupled nodes. Using (5) and (6) and making a standard Born–Markov approximation, we can derive a set of coupled quantum Langevin equations (QLEs) [38]. For each node we obtain

$$\dot{b}_i = \mathrm{i}[H_{\mathrm{node}}, b_i] - \frac{\gamma}{2}b_i - \sqrt{\gamma_{\mathrm{R}}}b_{i,\mathrm{in}}^{\mathrm{R}}(t) - \sqrt{\gamma_{\mathrm{L}}}b_{i,\mathrm{in}}^{\mathrm{L}}(t), \tag{7}$$

where $\gamma = \gamma_{\mathrm{R}} + \gamma_{\mathrm{L}}$ is the total decay rate of phonons into the waveguide. For side-coupled phonon cavities we would usually have $\gamma_{\mathrm{R}} = \gamma_{\mathrm{L}}$, but below we describe scenarios where the emission either to the left or to the right is effectively switched off. In equation (7) we have defined incoming fields (see figure 1(c))

$$b_{i,\mathrm{in}}^{\mathrm{L}} = \lim_{\epsilon\to 0}\Phi_{\mathrm{L}}(z_i+\epsilon), \quad b_{i,\mathrm{in}}^{\mathrm{R}} = \lim_{\epsilon\to 0}\Phi_{\mathrm{R}}(z_i-\epsilon), \tag{8}$$

which specify the left- and right-moving waveguide modes before they interact with b_i. Similarly, we introduce the scattered outgoing fields

$$b_{i,\mathrm{out}}^{\mathrm{L}} = \lim_{\epsilon\to 0}\Phi_{\mathrm{L}}(z_i-\epsilon), \quad b_{i,\mathrm{out}}^{\mathrm{R}} = \lim_{\epsilon\to 0}\Phi_{\mathrm{R}}(z_i+\epsilon). \tag{9}$$

The dynamics of the whole network is then described by the QLEs (7) together with the input–output relations at each node,

$$b_{i,\mathrm{out}}^{\mathrm{R,L}}(t) = b_{i,\mathrm{in}}^{\mathrm{R,L}}(t) + \sqrt{\gamma_{\mathrm{R,L}}}b_i(t), \tag{10}$$

and the free propagation

$$b_{i,\mathrm{in}}^{\mathrm{R}}(t) = b_{i-1,\mathrm{out}}^{\mathrm{R}}(t-\tau_{i,i+1}), \quad b_{i,\mathrm{in}}^{\mathrm{L}}(t) = b_{i+1,\mathrm{out}}^{\mathrm{L}}(t-\tau_{i,i+1}), \tag{11}$$

where $\tau_{i,i+1} = |z_{i+1} - z_i|/c$. Under realistic conditions we must also account for intrinsic phonon losses, backscattering and rethermalization, which we address below.

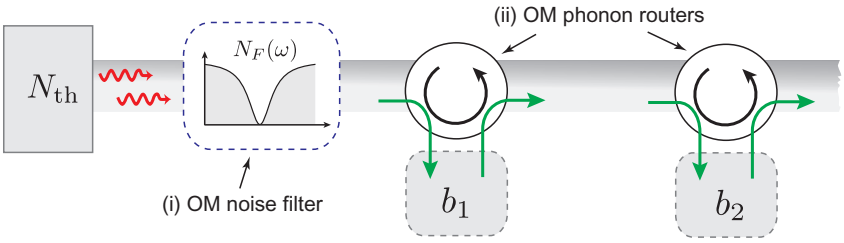

Figure 2. Basic setup illustrating the application of OM control techniques for implementing a directed quantum state transfer between two nodes through a thermal phonon network. (i) An OM noise filter is used to suppress incident thermal noise $\sim N_{\rm th}$ within a relevant transmission bandwidth. (ii) OM phonon routers ensure a directed emission and complete reabsorption of individual phonons at the second node. To achieve the reverse state transfer the directionality of the routers can be reversed, as described in more detail in section 5.

2.3. Optomechanical control techniques for phonon networks

The phonon network described above is formally equivalent to optical quantum networks and can, in principle, be used in a similar way to transfer quantum states from one node to another [29, 31]. However, in contrast to high-frequency optical fields, the thermal population $N_{\rm th} = (\exp(\hbar\omega_{\rm m}/k_{\rm B}T) - 1)^{-1}$ of the phonon modes is usually not negligible. For phonon frequencies in the MHz to GHz regime and temperatures $T \sim 0.1$–1 K, the number of thermal noise phonons in the waveguide will exceed the quantum signal encoded in a single phonon. In addition, as shown in figure 1(c), phonons emitted from a single side-coupled node will naturally propagate along two directions, i.e. $\gamma_{\rm L} = \gamma_{\rm R}$. In larger networks or 2D arrangements, the inability to route propagating phonons severely limits an efficient implementation of quantum communication protocols.

In the remainder of the paper, we consider an extended setup as shown in figure 2 and describe how the integration of additional OM control elements can be used to overcome these fundamental limitations of phononic networks. The two key ingredients in this setup are the following:

(i) an OM noise filter, which is used to suppress thermal noise within the relevant transmission bandwidth;

(ii) coherent OM phonon circulators or phonon routers, which allow for directed propagation and switchable routing of phonons through the network.

3. Optomechanical noise filters

In this section, we describe the application of OM laser cooling techniques to suppress thermal noise in an extended phononic quantum channel. Obviously, ground-state cooling of the whole network becomes inefficient as the system size increases, but it is also unnecessary, since usually only a few modes within a small bandwidth are used for transmitting quantum states. In the following, we consider a scenario as shown in figure 3, where a single laser-cooled mechanical resonator provides a 'cold sink', and within a certain frequency range suppresses the thermal

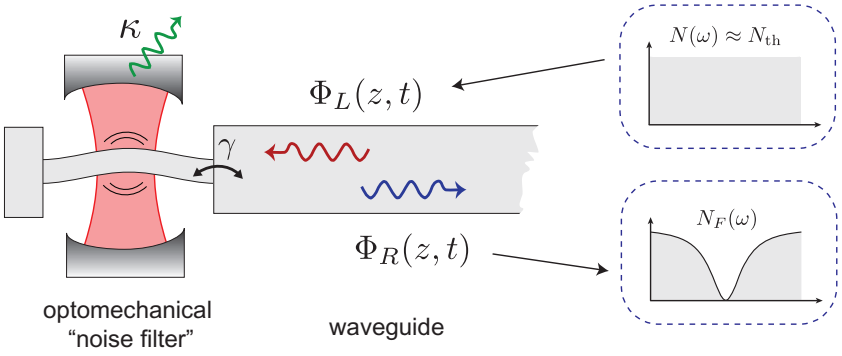

Figure 3. Setup for an OM noise filter (OM continuous mode cooling). A mechanical resonator is coupled to a continuous phonon waveguide (γ) and laser cooled via an optical cavity mode. Within a bandwidth $\sim\gamma$ around the mechanical frequency, the incident thermal noise can be efficiently suppressed, creating a dip in the filtered noise spectrum $N_{\rm F}(\omega)$ of the reflected waveguide modes.

noise of the reflected modes of a continuous waveguide (or the transmitted modes in the case of a side-coupled phonon cavity). A similar configuration has been previously proposed for realizing a traveling-wave photon-to-phonon converter, where under 'impedance-matched' conditions an incoming photon is converted into a traveling phonon and vice versa [25]. In this sense cooling of the waveguide can be interpreted as a mapping of the optical vacuum onto the phonon channel, while in turn mechanical noise is upconverted into optical photons leaving the system.

3.1. Single-mode cooling

Before addressing the suppression of thermal noise in extended phonon waveguides, let us first briefly review the standard scenario for OM cooling [39, 40], where the frequency $\omega_{\rm c}$ of an optical cavity mode is modulated by the displacement of a single mechanical mode. The optical cavity is driven by a coherent laser field of frequency $\omega_{\rm d} = \omega_{\rm c} + \delta$ and in a frame rotating with $\omega_{\rm d}$ the Hamiltonian for the OMS is given by

$$H_{\rm om} = -\delta a^\dagger a + \omega_{\rm m} b^\dagger b + g a^\dagger a (b + b^\dagger) + {\rm i}\,\mathcal{E}(a^\dagger - a). \tag{12}$$

Here the bosonic operators a and b represent the optical and mechanical modes, respectively, $\omega_{\rm m}$ is the mechanical oscillation frequency, g is the OM coupling constant and $\mathcal{E}$ is the strength of the external driving field. Terms rotating with the optical frequency have been neglected by a rotating wave approximation (RWA). The OM interaction, as described by the third term in equation (12), derives from a linear dependence of the optical resonance frequency on the position quadrature of the mechanical mode [41, 42]. Including dissipation through cavity decay and intrinsic mechanical losses, the dynamics of the OMS is described by the QLEs

$$\dot{a} = ({\rm i}\delta - \kappa)a - {\rm i}g a(b + b^\dagger) + \mathcal{E} - \sqrt{2\kappa}\,a_{\rm in}, \tag{13}$$

$$\dot{b} = (-{\rm i}\omega_{\rm m} - \gamma_0/2)b - {\rm i}g a^\dagger a - \sqrt{\gamma_0}\,b_{0,{\rm in}}, \tag{14}$$

where κ is the optical field decay rate and $\gamma_0 = \omega_{\rm m}/Q_0$ is the mechanical damping rate for an intrinsic mechanical quality factor Q_0. The δ-correlated operators $a_{\rm in}$ and $b_{0,{\rm in}}$ represent

the vacuum input noise of the optical field and the thermal mechanical noise, respectively. Within the relevant frequency range the latter is characterized by a non-vanishing equilibrium occupation number $\langle b_{0,\mathrm{in}}^{\dagger}(t) b_{0,\mathrm{in}}(t')\rangle = N_{\mathrm{th}}\delta(t-t')$.

In the limit of strong driving, the external field displaces both the optical and the mechanical modes by a large classical amplitude $\alpha = \langle a\rangle = \mathcal{E}/(\kappa - \mathrm{i}\delta(\alpha))$ and $\beta = \langle b\rangle = -g|\alpha|^2/\omega_{\mathrm{m}}$, where $\delta(\alpha) = \delta + 2g^2|\alpha|^2/\omega_{\mathrm{m}}$. For $|\alpha| \gg 1$, we can make a unitary transformation $a \to \alpha + a$ and $b \to \beta + b$ and linearize the OM coupling around the classical mean values,

$$H_{\mathrm{om}} \simeq -\delta a^{\dagger}a + \omega_{\mathrm{m}} b^{\dagger}b + g(\alpha a^{\dagger} + \alpha^{*}a)(b + b^{\dagger}), \tag{15}$$

where we have redefined $\delta(\alpha) \to \delta$. If the external driving field is (near) resonant with the red mechanical sideband of the optical cavity, i.e. if $\delta \simeq -\omega_{\mathrm{m}}$, and if $\omega_{\mathrm{m}} \gg \kappa, |g\alpha|$ we can make an RWA with respect to ω_{m} and obtain a beam-splitter Hamiltonian

$$H_{\mathrm{om}} \simeq H_{\mathrm{bs}} = (\omega_{\mathrm{m}} + \delta) b^{\dagger}b + g(\alpha b a^{\dagger} + \alpha^{*} b^{\dagger} a), \tag{16}$$

which describes a (near) resonant conversion of phonons into photons (and vice versa). Combined with the decay from the optical cavity, it allows for cooling: incident (noise) phonons are up-converted to photons and decay from the optical cavity.

The QLEs for the linearized OMS can be conveniently solved in the Fourier domain as outlined in more detail in appendix B. In the relevant weak coupling and sideband resolved regime ($|g\alpha| < \kappa \ll \omega_{\mathrm{m}} = -\delta$), we then obtain the standard result for the mechanical fluctuation spectrum,

$$\langle b^{\dagger}(\omega) b(\omega')\rangle \simeq \left[\frac{(\gamma_0 + \gamma_{\mathrm{op}})\bar{N}}{(\omega - \omega_{\mathrm{m}})^2 + (\gamma_0 + \gamma_{\mathrm{op}})^2/4}\right]\delta(\omega - \omega'), \tag{17}$$

where $\gamma_{\mathrm{op}} = 2|g\alpha|^2/\kappa$ is the optically induced mechanical damping rate and $\bar{N} = N_{\mathrm{th}}\gamma_0/(\gamma_0 + \gamma_{\mathrm{op}}) + \kappa^2/(4\omega_{\mathrm{m}}^2)$ the reduced steady-state resonator occupation number. In the following, we are interested in OMS where both $\gamma_{\mathrm{op}} \gg \gamma_0$ and single-mode ground-state cooling $\bar{N} < 1$ can be achieved.

3.2. Optomechanical cooling in a multi-mode system

The single-mode cooling scheme can be generalized to cool mechanical networks consisting of a few coupled resonators only one of which is OM cooled, as shown in figure 4(b). In this case the linearized OM Hamiltonian is given by

$$H_{\mathrm{om}} \simeq -\delta a^{\dagger}a + \sum_{j=1}^{N} \omega_{\mathrm{m}} b_j^{\dagger} b_j - \sum_{\langle i,j\rangle} K_{i,j}\left(b_i b_j^{\dagger} + b_i^{\dagger} b_j\right) + g\alpha\left(a^{\dagger} b_1 + a b_1^{\dagger}\right), \tag{18}$$

where the $K_{i,j}$ denote the nearest-neighbor couplings and we have already performed an RWA assuming that $K_{i,j}, g|\alpha|, \kappa \ll \omega_{\mathrm{m}}$. The resulting QLEs can be written as

$$\dot{a} = (\mathrm{i}\,\delta - \kappa)a - \mathrm{i}\,\alpha g b_1 - \sqrt{2\kappa}\,a_{\mathrm{in}}, \tag{19}$$

$$\dot{b}_1 = -(\mathrm{i}\,\omega_{\mathrm{m}} + \gamma_0/2) b_1 + \mathrm{i}\,K_{1,2} b_2 - \mathrm{i}\,g\alpha^{*} a - \sqrt{\gamma_0}\, b_{0,\mathrm{in}}^{(1)}, \tag{20}$$

$$\dot{b}_{1<j<N} = -(\mathrm{i}\,\omega_{\mathrm{m}} + \gamma_0/2) b_j + \mathrm{i}(K_{j-1,j} b_{j-1} + K_{j,j+1} b_{j+1}) - \sqrt{\gamma_0}\, b_{0,\mathrm{in}}^{(j)}, \tag{21}$$

$$\dot{b}_N = -(\mathrm{i}\,\omega_{\mathrm{m}} + \gamma_0/2) b_N + \mathrm{i}\,K_{N-1,N} b_{N-1} - \sqrt{\gamma_0}\, b_{0,\mathrm{in}}^{(N)}, \tag{22}$$

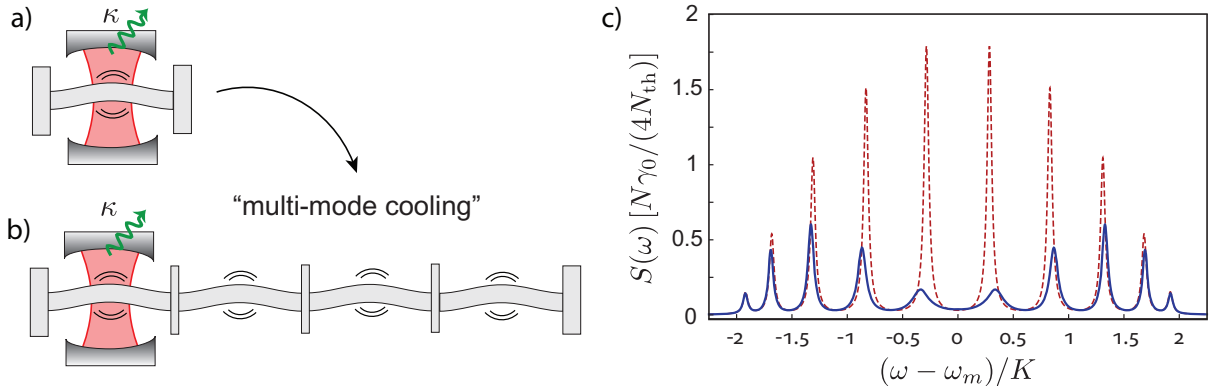

Figure 4. (a) Setup for OM cooling of a single mechanical mode and (b) its generalization to multiple coupled resonators. (c) The steady-state fluctuation spectrum $S(\omega)$ as defined in the text is plotted for the b_{10} mode in an array of $N = 10$ resonators, assuming that the b_1 mode is OM cooled. The dashed line shows the result in the absence of OM cooling, i.e. $g|\alpha| = 0$, while the solid line corresponds to $g|\alpha|/K = 0.5$. The other parameters for this plot are $\delta = -\omega_{\rm m}$, $\gamma_0/K = 0.05$ and $\kappa/K = 0.5$.

where the $b^{(j)}_{0,\rm in}$ are mutually uncorrelated noise operators associated with intrinsic mechanical damping of each mode.

In figure 4(c) we plot the correlation spectrum $\langle b^\dagger_N(\omega) b_N(\omega')\rangle = S(\omega)\delta(\omega-\omega')$ for a chain of $N = 10$ resonators with $K_{i,i+1} = K$ assuming that the b_1 mode is optically cooled. For reference the dashed line shows the undamped case $g\alpha = 0$. In this case the heights of the peaks at frequencies $\omega_n = \omega_{\rm m} - 2K\cos(n\pi/(N+1))$ are given by $S(\omega_n) = (4N_{\rm th}/\gamma_0)|c_n(N)|^2$, where $c_n(j) = \sqrt{2/(N+1)}\sin(nj\pi/(N+1))$ are the normalized mode distributions. When the OM coupling is turned on, the peaks are broadened and their height is reduced, which corresponds to an overall cooling of the individual eigenmodes. However, we see that cooling occurs in a highly non-uniform way and only the few modes close to the cavity resonance are cooled efficiently. While the details depend on the ratios between K, $g|\alpha|$ and κ, we find that this behavior is quite generic and a precursor to the features we identify in the following for the continuous waveguide limit.

3.3. Optomechanical cooling of a mode continuum

Starting from the multi-mode setting shown in figure 4(b), let us now address the limit $N \to \infty$ of a continuous mode waveguide as depicted in figure 3 by retaining the OM coupling to the first mode $b \equiv b_1$, but describing the other phonon modes $b_{j>1}$ in terms of continuous left- and right-propagating fields $\Phi_{\rm L,R}(z)$. If $K_{1,2} \ll K_{i,i+1} \equiv K$, we can adapt the input–output formalism introduced in section 2 to model the coupling between the localized mode b and the rest of the waveguide in terms of the scattering relation

$$b_{\rm out}(t) = b_{\rm in}(t) + \sqrt{\gamma}\, b(t). \tag{23}$$

Here $b_{\rm in}(t) = \Phi_{\rm L}(z \to 0, t)$ and $b_{\rm out}(t) = \Phi_{\rm R}(z \to 0, t)$ are the incident and reflected waveguide fields and $\gamma \approx K^2_{1,2}/K$ is the characteristic phonon decay rate into the waveguide.

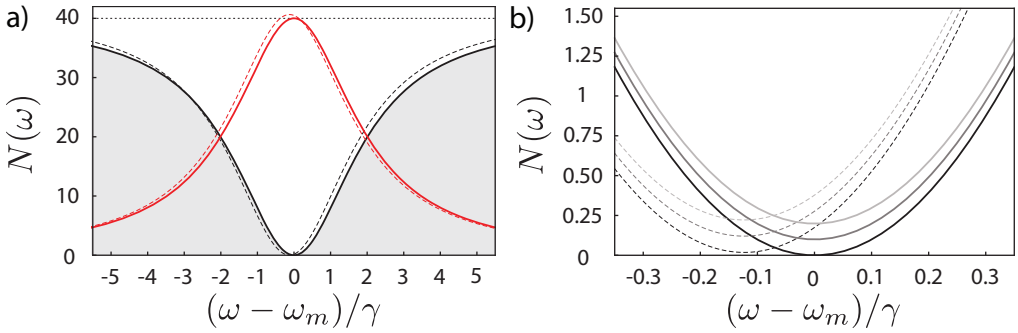

Figure 5. Detailed results for OM noise filtering. (a) Filtered phononic noise spectrum $N_{\rm F}(\omega)$ (black lines) and the corresponding photonic output spectrum (red lines), with the beam-splitter Hamiltonian (16) (solid lines) and with the full linearized Hamiltonian (15) (dashed lines). The parameters are $\omega_{\rm m}/\gamma = 1200$, $\gamma_0 = 0$, $\kappa/\gamma = 300$, $g|\alpha| = \sqrt{(\gamma+\gamma_0)\kappa/2}$ and $N_{\rm th} = 40$. (b) Dip of the filtered noise spectrum $N_{\rm F}(\omega)$ for different values of the intrinsic mechanical damping rate $\gamma_0/\gamma = 0,\ 0.0025,\ 0.005$.

Ignoring other, intrinsic loss channels for the moment, we obtain

$$\dot{a} = (\mathrm{i}\delta - \kappa)a - \mathrm{i}\alpha g(b + b^\dagger) - \sqrt{2\kappa}a_{\rm in}, \tag{24}$$

$$\dot{b} = -(\mathrm{i}\omega_{\rm m} + \gamma/2)b - \mathrm{i}g(\alpha a^\dagger + \alpha^* a) - \sqrt{\gamma}b_{\rm in}, \tag{25}$$

for the linearized OM dynamics of the local mode and we see that the problem of cooling a continuous waveguide is formally identical to the single-mode cooling considered above. However, instead of looking at the occupation of the local mode b we are now interested in the spectrum of the reflected waveguide field $b_{\rm out}(t)$, given a thermal incident field $\langle b_{\rm in}^\dagger(t) b_{\rm in}(t')\rangle = N_{\rm th}\delta(t-t')$. To do so, we solve the QLEs in Fourier space and write the result as

$$\vec{A}_{\rm out}(\omega) = \mathcal{S}(\omega)\vec{A}_{\rm in}(\omega), \tag{26}$$

where $\vec{A}_j = (a_j(\omega), a_j^\dagger(-\omega), b_j(\omega), b_j^\dagger(-\omega))^{\rm T}$ with $j =$ 'in', 'out'. The matrix $\mathcal{S}(\omega)$ is a 4×4 scattering matrix and a more detailed derivation of equation (26) is given in appendix B. For given input noise correlations $C_{\rm in}(\omega,\omega') = \langle \vec{A}_{\rm in}(\omega) \otimes \vec{A}_{\rm in}^{\rm T}(\omega')\rangle$, we obtain the output correlation matrix $C_{\rm out}(\omega,\omega') = \langle \vec{A}_{\rm out}(\omega) \otimes \vec{A}_{\rm out}^{\rm T}(\omega')\rangle = \mathcal{S}(\omega)C_{\rm in}(\omega,\omega')\mathcal{S}^{\rm T}(\omega')$.

3.3.1. Optomechanical noise filters. The quantity that we are interested in is the filtered noise spectrum $N_{\rm F}(\omega)$ of the reflected field, which is defined by

$$\langle b_{\rm out}^\dagger(\omega) b_{\rm out}(\omega')\rangle = N_{\rm F}(\omega)\delta(\omega-\omega'). \tag{27}$$

Figure 5(a) shows the typical frequency dependence of $N_{\rm F}(\omega)$. As expected, we see a strong suppression of thermal noise around the mechanical frequency $\omega_{\rm m}$. For $\delta = -\omega_{\rm m}$ and under the condition $|g\alpha| < \kappa \ll \omega_{\rm m}$, the dynamics of the OMS is well approximated by the beam-splitter Hamiltonian (16) and we obtain

$$N_{\rm F}(\omega) \simeq N_{\rm th}\left(1 - \frac{4\kappa^2\gamma_{\rm op}\gamma}{\kappa^2(\gamma_{\rm op}+\gamma)^2 + (\gamma-2\kappa)^2(\omega-\omega_{\rm m})^2 + 4(\omega-\omega_{\rm m})^4}\right). \tag{28}$$

We see that, under these approximations, the 'impedance matching' condition $\gamma_{\rm op} = \gamma$ [25] results in a complete cancellation $N_{\rm F}(\omega = \omega_{\rm m}) = 0$ of the reflected noise on resonance. In this case the optical decay rate matches the mechanical waveguide coupling and the OMS acts effectively as a double-sided phonon cavity with the thermal mechanical bath on the one side and the optical $T = 0$ bath on the other side.

Under realistic conditions the noise cancellation described by equation (28) will not be perfect, and to account for various imperfections in the system, we assume in our discussion below a spectrum of the form

$$N_{\rm F}(\omega) = N_{\rm th} - (N_{\rm th} - N_0)\frac{\tilde{\gamma}^2}{(\omega - \tilde{\omega}_{\rm m})^2 + \tilde{\gamma}^2}, \tag{29}$$

where $\tilde{\gamma}$ and $\tilde{\omega}_{\rm m}$ now include small corrections of the width and the center of the dip and N_0 is a non-vanishing noise floor. Intrinsic limitations that lead to a finite N_0 are already contained in the full OM interaction itself, where for any finite $\omega_{\rm m}$ off-resonant Stokes-scattering terms in the linearized Hamiltonian (15) induce corrections to the ideal beam-splitter interaction. However, as shown in figure 5(b), by accounting for these effects up to second order in $1/\omega_{\rm m}$ we only obtain a small shift of the spectral dip $\tilde{\omega}_{\rm m} \simeq \omega_{\rm m} - g^2|\alpha|^2/(2\omega_{\rm m})^2$ and an offset $N_0 \simeq |g\alpha|^2/(4\omega_{\rm m}^2)$, which is negligible under the weak coupling conditions mentioned above. A more crucial limitation for the OM noise filter arises from intrinsic mechanical losses γ_0 of the localized mechanical mode, which can be accounted for by introducing an additional decay rate γ_0 and the associated noise operator $b_{0,\rm in}(t)$ in the QLE (25) (see appendix B). This leads to a finite $N_0 \simeq 4N_{\rm th}\gamma\gamma_0/(\gamma_{\rm op} + \gamma + \gamma_0)^2$. This means that, while for the optimized case with $\gamma = \gamma_0 + \gamma_{\rm op}$ the local mode b can be highly excited, also the condition $\gamma_0 N_{\rm th}/\gamma_{\rm op} \ll 1$ must be fulfilled to achieve good noise filtering.

3.3.2. Propagation losses and scattering. The spectrum $N_{\rm F}(\omega)$ determines the mechanical noise of the outgoing displacement field $b_{\rm out}(t) \equiv \Phi_{\rm R}(z \to 0, t)$ immediately after the OM device and for an ideal phonon waveguide this noise spectrum will be the same at all positions $z > 0$. However, in a realistic setting, scattering losses in the waveguide and the associated noise lead to a rethermalization of the noise spectrum and $N_{\rm F}(\omega) \to N_{\rm F}(\omega, z)$. For an approximately linear dispersion relation, the propagation of the outgoing field can be modeled by

$$\left(\frac{\partial}{\partial t} + c\frac{\partial}{\partial z}\right)\Phi_{\rm R}(z,t) = -\left(i\tilde{\omega}_0 + \frac{c}{2l_\gamma}\right)\Phi_{\rm R}(z,t) - \frac{c}{\sqrt{l_\gamma}}\Phi_{\rm th}(z,t), \tag{30}$$

where l_γ is the phonon mean free path in the waveguide and $\Phi_{\rm th}(z,t)$ is a thermal noise field with $\langle\Phi_{\rm th}^\dagger(z,t)\Phi_{\rm th}(z',t')\rangle = N_{\rm th}\delta(z-z')\delta(t-t')$. In appendix A.1 we outline a microscopic derivation of this result for a coupled mechanical resonator array, where $l_\gamma = c/\gamma_0$ can be connected to the intrinsic damping rate γ_0 of the individual resonators in the array. For $z > 0$ and in a frame rotating with $\tilde{\omega}_0$, we obtain

$$\Phi_{\rm R}(z,t) = e^{-\frac{z}{2l_\gamma}}\Phi_{\rm R}\left(0, t - \frac{z}{c}\right) - \frac{1}{\sqrt{l_\gamma}}\int_0^z dz'\, e^{-\frac{(z-z')}{2l_\gamma}}\Phi_{\rm th}\left(z', t - \frac{(z-z')}{c}\right), \tag{31}$$

and from this result we can derive the full noise spectrum along the waveguide

$$N_{\rm F}(\omega, z) = e^{-\frac{z}{l_\gamma}}N_{\rm F}(\omega, 0) + N_{\rm th}\left(1 - e^{-\frac{z}{l_\gamma}}\right). \tag{32}$$

This result describes the rethermalization of the noise dip on a length scale given by the phonon mean free path. For the relevant distances $z \ll l_\gamma$, the noise spectrum can still be described by the Lorentzian shape given in equation (29), but the noise floor $N_0(z) \simeq N_0 + (z/l_\gamma)N_{\rm th}$ increases linearly with the distance to the OM noise filter. Note that similar quantitative conclusions follow from the standard approach of treating propagation losses in terms of a series of beam splitters [25, 38], but the present analysis also provides a direct connection to the underlying microscopic phonon scattering mechanism.

To the extent that the scatterers are linear, phonon backscattering gives rise to small overall losses, which are on an equal footing with the thermalization discussed above.

4. Quantum state transfer in a thermal phonon network

We now return to our original goal of implementing a quantum state-transfer protocol between two qubits via an extended and thermally occupied phononic channel. For a simplified discussion we consider in the following the state transfer between two nodes assuming a unidirectional coupling, where $\gamma \equiv \gamma_{\rm R}$, $\gamma_{\rm L} = 0$ and $b_{i,\rm in/out} \equiv b^{\rm R}_{i,\rm in/out}$ as shown in figure 2. In section 5, we describe how this condition can be realized using phonon routers.

4.1. A tunable qubit network

As a first step we describe the implementation of an effective qubit network with tunable qubit–waveguide couplings $\Gamma_{1,2}(t)$ by eliminating the dynamics of the local phonon modes. We start from the full set of QLEs, which, for each node $j = 1, 2$, derive from the Hamiltonian in (2) and are given by

$$\dot\sigma^j_- = -{\rm i}\Delta_{\rm q}(t)\sigma^j_- + {\rm i}\,\lambda_j(t)\sigma^j_z b_j, \tag{33}$$

$$\dot\sigma^j_z = -2{\rm i}\,\lambda_j(t)(\sigma^j_+ b_j - b^\dagger_j\sigma^j_-), \tag{34}$$

$$\dot b_j = -{\rm i}\,\omega_{\rm m} b_j - \frac{\gamma}{2} b_j - {\rm i}\,\lambda_j(t)\sigma^j_- - \sqrt{\gamma} b_{j,\rm in}. \tag{35}$$

The input–output relations are

$$b_{j,\rm out}(t) = b_{j,\rm in}(t) + \sqrt{\gamma} b_j(t) \quad \text{and} \quad b_{2,\rm in}(t) = b_{1,\rm out}(t - \tau_{12}), \tag{36}$$

where $b_{1,\rm in}(t) \equiv b_{\rm in}(t)$ describes the incident waveguide field before interacting with the first node. Hereafter, we absorb the retardation time τ_{12} by redefining time-shifted operators and control fields for the second node [38] and for simplicity we focus on the resonant case in which $\Delta^j_{\rm q}(t) = \omega_{\rm m}$.

We are interested in the regime in which the decay γ of the the local phonon modes into the waveguide is fast compared to the coupling $\lambda(t)$. This allows us to adiabatically eliminate the phonon modes and to derive an effective description in terms of the qubit degrees of freedom only. In the frame rotating with $\omega_{\rm m}$ and to lowest order in λ, (35) can be solved to give

$$b_j(t) \simeq -\frac{2{\rm i}\,\lambda_j(t)}{\gamma}\sigma^j_-(t) - \sqrt{\gamma}\int_{-\infty}^{t} {\rm d}s\, {\rm e}^{-\frac{\gamma}{2}(t-s)}\, {\rm e}^{{\rm i}\,\omega_{\rm m} s} b_{j,\rm in}(s). \tag{37}$$

After reinserting this expression into equations (33) and (34), we obtain

$$\dot{\sigma}_-^j = -\frac{\Gamma_j(t)}{2}\sigma_-^j - \sqrt{\Gamma_j(t)}\sigma_z^j B_{j,\mathrm{in}}, \tag{38}$$

$$\dot{\sigma}_z^j = -\Gamma_j(t)\left(\mathbb{1} + \sigma_z^j\right) + 2\sqrt{\Gamma_j(t)}\left(\sigma_+^j B_{j,\mathrm{in}} + B_{j,\mathrm{in}}^\dagger \sigma_-^j\right). \tag{39}$$

Here $\Gamma_j(t) = 4\lambda_j^2(t)/\gamma$ are tunable qubit decay rates and

$$B_{j,\mathrm{in}}(t) = \frac{\mathrm{i}\gamma}{2}\int_{-\infty}^{t} \mathrm{d}s\, \mathrm{e}^{-\frac{\gamma}{2}(t-s)}\, \mathrm{e}^{\mathrm{i}\omega_m s} b_{j,\mathrm{in}}(s), \tag{40}$$

the associated effective noise operators which on the timescale γ^{-1} obey $[B_{j,\mathrm{in}}(t), B_{j,\mathrm{in}}^\dagger(t')] \approx \delta(t-t')$. Provided that $\lambda(t)$ and $\sigma_-^1(t)$ also vary slowly on this time scale, we find that

$$B_{2,\mathrm{in}}(t) \simeq -B_{1,\mathrm{in}}(t) + \sqrt{\Gamma_1(t)}\sigma_-^1(t). \tag{41}$$

Thus, we obtain a new set of effective quantum network equations for the qubit operators with tunable decay rates $\Gamma_j(t)$. We emphasize that while in the following this effective description allows a simplified discussion of the state-transfer protocol, it is not necessary to consider the regime $\lambda \ll \gamma$ and a perfect state transfer can also be achieved using the full model [29].

4.2. Quantum state transfer through a phonon channel

Our goal is to implement a quantum state transfer between the two qubits, i.e.

$$|\psi_0\rangle = (\alpha|0\rangle_1 + \beta|1\rangle_1)|0\rangle_2 \to |0\rangle_1(\alpha|0\rangle_2 + \beta|1\rangle_2), \tag{42}$$

which is achieved via coherent emission and reabsorption of a single phonon in the waveguide. A solution to this problem was first described for optical networks [29], where it has been shown that by identifying appropriate pulses $\Gamma_j(t)$, a perfect quantum state transfer can be implemented. Let us briefly summarize the main idea behind this scheme, for the moment assuming zero temperature. In this case the waveguide is initially in the vacuum state $|\mathrm{vac}\rangle$ and the dynamics of the whole system can be restricted to the zero- and one-excitation subspace. Then, for an initial two-qubit state $|\psi_0\rangle$, we can define the amplitudes $v_j(t) = \langle \mathrm{vac}|\langle 0_1, 0_2|\sigma_-^j(t)|\psi_0\rangle|\mathrm{vac}\rangle$. From the QLEs (38) and (39) and the input–output relation (41), it follows that these amplitudes evolve according to

$$\dot{v}_1(t) = -\frac{\Gamma_1(t)}{2}v_1(t), \tag{43}$$

$$\dot{v}_2(t) = -\frac{\Gamma_2(t)}{2}v_1(t) - \sqrt{\Gamma_1(t)\Gamma_2(t)}v_1(t), \tag{44}$$

and for initial amplitudes $v_j(t_0)$, the general solutions is given by

$$v_1(t) = \mathcal{G}_1(t, t_0)v_1(t_0), \tag{45}$$

$$v_2(t) = \mathcal{G}_2(t, t_0)v_2(t_0) + \mathcal{T}(t, t_0)v_1(t_0). \tag{46}$$

Here $\mathcal{G}_j(t,t_0)=\mathrm{e}^{-\int_{t_0}^{t}\mathrm{d}s\,\Gamma_j(s)/2}$ and

$$\mathcal{T}(t,t_0)=-\int_{t_0}^{t}\mathrm{d}t'\,\mathcal{G}_2(t,t')\sqrt{\Gamma_1(t')\Gamma_2(t')}\mathcal{G}_1(t',t_0) \tag{47}$$

is the state-transfer amplitude. For the initial state given in equation (42), $v_2(t_0)=0$, and therefore a perfect transfer is achieved if at some final time t_f the amplitudes approach

$$\mathcal{G}_1(t_\mathrm{f},t_0)\to 0 \quad \text{and} \quad |\mathcal{T}(t_\mathrm{f},t_0)|\to 1. \tag{48}$$

While the first condition is easily fulfilled for sufficiently long but otherwise arbitrary pulses, satisfying the second one requires control over their shape. Perfect state transfer is only possible if the total number of excitations is conserved, i.e. if no population gets lost from the one-excitation subspace. This means that the norm $\mathcal{G}_1^2(t,t_0)+\mathcal{T}^2(t,t_0)=1$ for all times, which after taking the time derivative of this condition yields

$$\sqrt{\Gamma_1(t)}v_1(t)+\sqrt{\Gamma_2(t)}v_2(t)=0. \tag{49}$$

This result also follows from the requirement that the total scattered field after the second node vanishes at all times, i.e. $B_{2,\mathrm{out}}(t)|\psi_0\rangle|\mathrm{vac}\rangle=0$. Therefore equation (49) is often referred to as the *dark-state condition*.

A set of pulses $\Gamma_1(t)$ and $\Gamma_2(t)$ that realize a perfect state transfer can always be found numerically by choosing $\Gamma_1(t)$ such that $\mathcal{G}_1(t_\mathrm{f},t_0)\to 0$ and then solve equations (43) and (44) iteratively, choosing $\Gamma_2(t)$ at each time such that the dark-state condition (49) is fulfilled. Further, simple analytical expressions for pulses that realize a perfect state transfer may be obtained from a time-inversion argument [29]. Without loss of generality, we can assume that $[t_\mathrm{f},t_0]=[-\tau_\mathrm{p}/2,\tau_\mathrm{p}/2]$, where τ_p is the pulse length. A control pulse $\Gamma_1(t)$ for the first qubit gives rise to a wave packet $a(t)=\sqrt{\Gamma_1(t)}\mathcal{G}_1(t,t_0)v_1(t_0)$ in the waveguide. For reasons of time-inversion symmetry, the inverted wave packet $a(-t)$ is fully absorbed if the reverse pulse $\Gamma_1(-t)$ is applied. This implies that, in the special case of a time-symmetric wave packet $a(t)=a(-t)$, the wave packet generated at the first node will be fully absorbed if we choose $\Gamma_2(t)=\Gamma_1(-t)$. Describing the symmetric wave packet by the differential equation $\dot{a}(t)=g(t)a(t)$, where $g(t)$ is anti-symmetric $g(t)=-g(-t)$, one can derive the following differential equation for the pulse-shape $\Gamma_1(t)$ from (43) [43]:

$$\dot{\Gamma}_1=\Gamma_1^2+2g(t)\Gamma_1. \tag{50}$$

For the simplest choice of $g(t)$, i.e. $g(t)=\mathrm{sign}(t)(\Gamma_\mathrm{max}/2)$, where Γ_max is the maximal decay rate, the solution reads

$$\Gamma_1(t)=\begin{cases}\left(\frac{\mathrm{e}^{-\Gamma_\mathrm{max}t}}{2-\mathrm{e}^{-\Gamma_\mathrm{max}t}}\right)\Gamma_\mathrm{max} & \text{if} \quad t<0\\ \Gamma_\mathrm{max} & \text{if} \quad t\geqslant 0\end{cases} \quad \text{and} \quad \Gamma_2(t)=\Gamma_1(-t). \tag{51}$$

We will use this specific pulse shape for our numerical examples discussed below.

4.3. State transfer through a noisy quantum channel

Now we consider the same state-transfer problem but in the case when the in-field of the quantum channel is characterized by a non-vanishing noise spectrum $\langle B_\mathrm{in}^\dagger(\omega)B_\mathrm{in}(\omega')\rangle=N(\omega)\delta(\omega-\omega')$, which can be either a flat thermal background $N(\omega)=N_\mathrm{th}$ or the filtered noise dip $N(\omega)\simeq N_\mathrm{F}(\omega)$ as discussed in section 3.3.

4.3.1. Effective thermal occupation number. In the presence of thermal excitations in the quantum channel we must necessarily go beyond the single excitation subspace and a closed analytic solution to the state-transfer problem is no longer available. To gain more intuition on the impact of noise on the state-transfer fidelity, let us first consider a single qubit. We assume that at time $t = t_0$ the qubit is prepared in its ground state and we then switch on the coupling to the waveguide $\Gamma_1(t)$, for example, using the pulse shape defined in equation (51). In the regime where the noise amplitude is low, $N(\omega) \ll 1$, we can linearize the QLEs (38) and (39) and obtain for the final qubit excitation $\langle \sigma_+^1(t_f)\sigma_-^1(t_f)\rangle \simeq N_{\rm eff} \ll 1$, where

$$N_{\rm eff} = \int_{t_0}^{t_f} {\rm d}t_1 {\rm d}t_2 \sqrt{\Gamma_1(t_1)\Gamma_1(t_2)}\mathcal{G}_1(t_f, t_1)\mathcal{G}_1(t, t_2)\langle B_{\rm in}^\dagger(t_1)B_{\rm in}(t_2)\rangle. \tag{52}$$

In the case of incident δ-correlated thermal noise and assuming that the pulse duration is sufficiently long, i.e. $t_f - t_0 \gg \Gamma_{\rm max}^{-1}$, we find that $N_{\rm eff} = N_{\rm th}$. This means that during the state transfer an erroneous excitation or de-excitation probability for the qubits of $\sim N_{\rm th}$ can be expected.[5] In turn, for the filtered noise spectrum $N_{\rm F}(\omega)$ defined in equation (29) we obtain

$$N_{\rm eff} = \int_{-\infty}^{\infty} {\rm d}\omega\, |F(\omega)|^2 N_{\rm F}(\omega) \simeq \frac{2\gamma N_0 + \Gamma_{\rm max} N_{\rm th}}{2\gamma + \Gamma_{\rm max}}, \tag{53}$$

where in general $F(\omega) = \frac{1}{\sqrt{2\pi}} \int_{t_0}^{t_f} {\rm d}t {\rm e}^{{\rm i}\omega t} \sqrt{\Gamma_1(t)}\mathcal{G}_1(t_f, t)$ and the integral in equation (53) has been evaluated for the pulse shape given in equation (51). This shows that using the OM noise filter to clean the waveguide, the effective occupation number can be considerably reduced compared to $N_{\rm th}$, assuming that $N_0 \ll 1$ and that the bandwidth of the transfer pulse fits within the noise dip. This is illustrated in figure 6, where we plot the spectral overlap between $|F(\omega)|^2$ and $N_{\rm F}(\omega)$ and the resulting $N_{\rm eff}$ for different ratios $\gamma/\Gamma_{\rm max}$.

4.3.2. Discussion. To verify our approximate analytic predictions we convert the cascaded QLEs into an equivalent cascaded master equation [38] and simulate the full state transfer numerically. Since a master equation for the two qubits can only be derived for δ-correlated noise, we include the OM noise filter as a third subsystem to emulate the spectral variations of the incident noise, as outlined in appendix C. In figure 6(c) and (d) we simulate the transfer of a single-qubit excitation from node 1 to node 2 and compare the case of a thermal quantum channel where $N(\omega) = N_{\rm th}$ to the case when the OM noise filter is switched on and $N(\omega) = N_{\rm F}(\omega)$. We see that even for $N_{\rm th} = 0.5$ the thermal noise in a phonon quantum network already almost completely washes out the transferred signal, while in combination with the noise filter a high-fidelity state transfer is still possible. In figure 6(d) we also compare the full numerical results with a master equation for the qubits only, assuming a δ-correlated noise with an effective occupation number $N_{\rm eff}$. We find that apart from small corrections when pulses are switched on and off, this reduced model describes the state transfer very accurately, which shows that, indeed, $N_{\rm eff}$ is the relevant parameter for a quantum channel with a filtered noise spectrum.

As a specific example, we consider a potential realization of phonon networks using the on-chip OM structures discussed in [25]. We assume local phonon modes of frequency $\omega_{\rm m} = 2\pi \times 4\,{\rm GHz}$ and a decay into the waveguide of $\gamma = 2\pi \times 25\,{\rm MHz}$. For a quality factor

[5] Of course, for larger $N_{\rm th}$ the nonlinearity of the qubit must be taken into account.

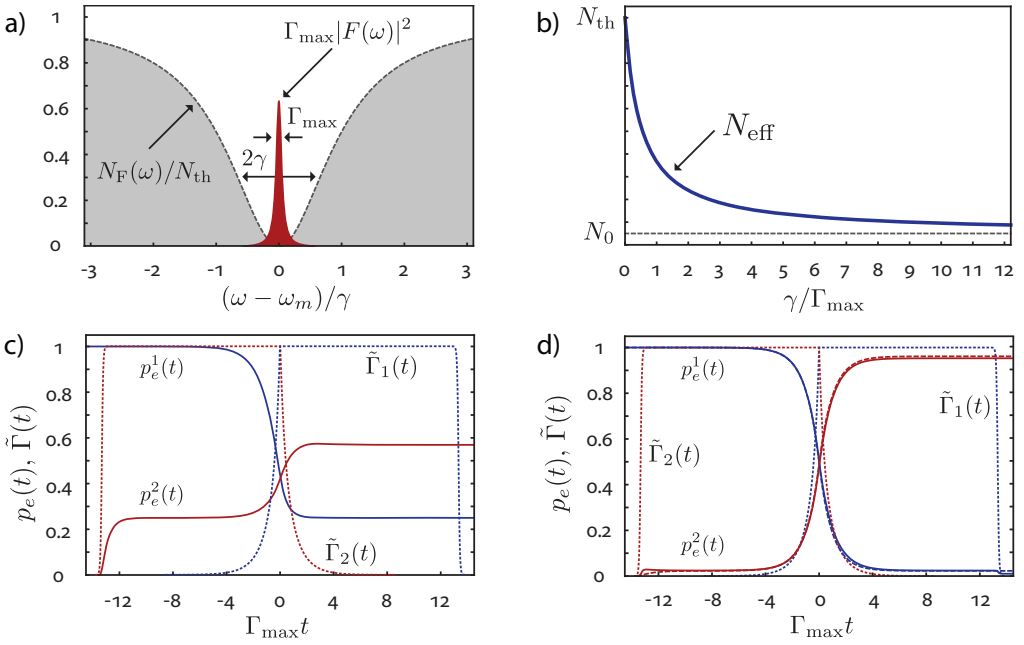

Figure 6. Quantum state transfer through a noisy channel. (a) Spectral overlap of the transfer pulse $|F(\omega)|^2$ and the filtered noise spectrum $N_{\rm F}(\omega)$ for $N_0 = 0$ and $\Gamma_{\max}/\gamma = 0.10$. (b) Effective occupation number $N_{\rm eff}$ as a function of $\gamma/\Gamma_{\max}$ for $N_0/N_{\rm th} = 0.05$. (c) Numerical simulation of a quantum state transfer in the presence of thermal noise with $N_{\rm th} = 0.5$. (d) The same state transfer with the OM noise filter switched on and $\Gamma_{\max}/\gamma = 0.10$. In both plots the blue and red solid lines show the excited state populations $p_{\rm e}^i(t) = \langle\sigma_+^i(t)\sigma_-^i(t)\rangle$ for qubits 1 and 2, respectively. The dotted lines show the corresponding pulse shapes $\tilde{\Gamma}_i(t) = \Gamma_i(t)/\Gamma_{\max}$ as defined in equation (51), but with cut-offs. In (d) the dashed line shows the results obtained from a two-qubit cascaded master equation with an effective thermal occupation number $N_{\rm eff}$.

$Q_0 = 10^6$ the intrinsic decoherence rate is $\gamma_0 = 2\pi \times 4\,\text{kHz}$. For these parameters we plot in figure 7 the fidelity $\mathcal{F}$ for transferring the superposition state $|\psi\rangle = (|0\rangle + |1\rangle)/\sqrt{2}$ between two nodes of a phonon network as a function of $N_{\rm th}$ and for different effective qubit decay rates $\gamma_0 \ll \Gamma_{\max} < \gamma$. For the numerical simulations we have used the effective model with $N_{\rm eff}$ as obtained in equation (53) and with $N_0 = \gamma_0 N_{\rm th}/\gamma$. The fidelity is defined as the overlap between the target state and the actual state after the transfer, i.e. $\mathcal{F} = \text{Tr}\{\rho_{\rm tar}\rho(t_{\rm f})\}$. We see that compared to the case where no cooling is applied and the fidelity already drops significantly for $N_{\rm th} \sim 0.1$, the presence of the OM noise filter can push this bound to much larger occupation numbers. In particular, in the example considered here, this means that instead of requiring temperatures of $T \leqslant 100\,\text{mK}$, the OM cooling scheme allows the implementation of high-fidelity state-transfer protocols at much more convenient liquid helium temperatures $T = 4\,\text{K}$ where $N_{\rm th} \sim 20$. Note that for the assumed value of $\Gamma_{\max} = 10^{-2}\gamma = 2\pi \times 250\,\text{kHz}$, the total transfer time of $\sim 1\,\mu\text{s}$ is compatible with decoherence times that are achievable with various different solid-state qubits. A few specific examples will be discussed in section 6.

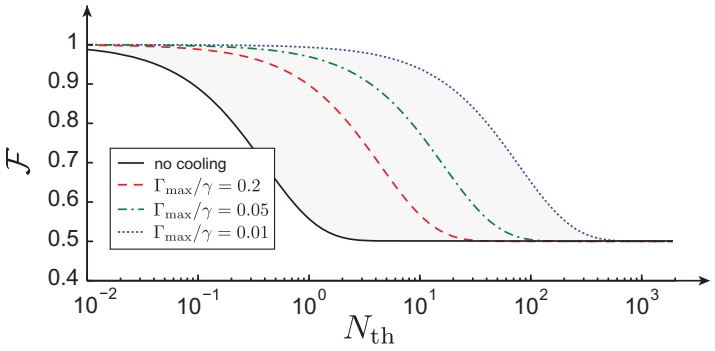

Figure 7. Quantum state-transfer fidelity $\mathcal{F}$ for a superposition state $|\psi\rangle = (|0\rangle + |1\rangle)/\sqrt{2}$ as a function of the thermal occupation $N_{\rm th}$ of the waveguide and different values of $\Gamma_{\max}$. For this plot we have used the pulse shape given in equation (51) and assumed that $\gamma_0/\gamma = 1.6 \times 10^{-4}$.

5. Phonon routers

In the previous sections, we have studied the transfer of single excitations through a thermal phonon network assuming that two nodes are coupled in a unidirectional way. This situation is applicable only to specific setups, for example, when the two nodes are located at the two ends of a single waveguide. In general, the emission of phonons into left- *and* right-propagating modes, reflection and interference effects, or imperfect routing of phonons through multi-port junctions in a 2D setting will limit the implementation of efficient state-transfer protocols in larger networks. In optical networks, many of these problems can be overcome by using optical circulators and optical isolators for the directional routing of photons. In the context of OMS it has already been suggested to use the intrinsic nonlinearity of OM interactions to induce non-reciprocal effects for light [35, 36]. In the following, we describe a related scheme, which allows us to engineer coherent non-reciprocal effects for phonons, where the directionality is simply imposed by the phase difference between two optical driving fields.

5.1. A three-port phonon circulator

To illustrate the basic idea of a non-reciprocal phonon device let us consider the minimal setting of a three-port circulator as shown in figure 8(a). The localized phonon modes $b_{j=1,2,3}$ are mutually tunnel coupled with a strength $|t|$ and coupled to phonon waveguides with a decay rate γ. The Hamiltonian is given by

$$H_{\rm circ} = \sum_i \omega_{\rm m} b_i^\dagger b_i + t\left(b_1 b_2^\dagger e^{i\varphi} + b_2 b_3^\dagger + b_3 b_1^\dagger + \text{H.c.}\right), \tag{54}$$

assuming that the resonator frequencies $\omega_{\rm m}$ are all equal. The crucial term in this setup is a complex tunneling amplitude $te^{i\varphi}$ between two of the resonators, which cannot be absorbed into local redefinitions of the b_i. Therefore, this phase can be associated with an effective magnetic field for the phonon modes. Previously, such a setting was described for superconducting microwave cavities, where the effective magnetic field can be engineered using superconducting qubits and external fluxes [44, 45]. Below we describe a non-magnetic approach to achieve this complex hopping amplitude in OMS.

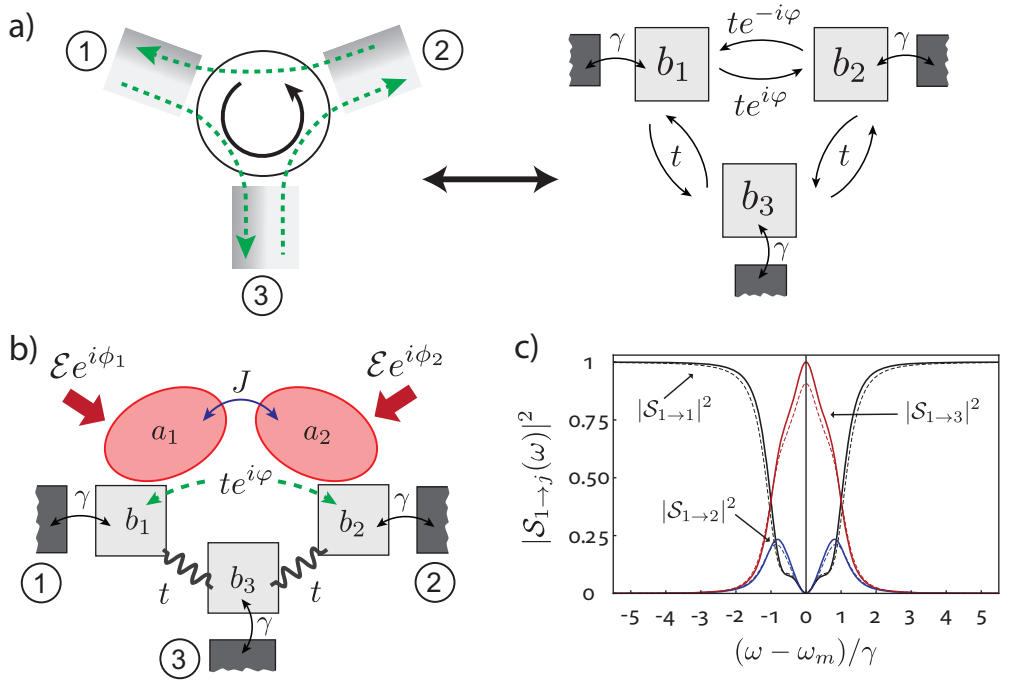

Figure 8. A phonon circulator. (a) General scheme for realizing a three-port circulator based on three coupled phonon cavities, where one of the tunneling amplitudes is complex. A cyclic scattering of phonons between the three ports is achieved for $t=\gamma/2$ and $\varphi=\pi/2$. (b) A two-mode OM setup for implementing an effective non-reciprocal tunneling amplitude $te^{i\varphi}$. The two coupled optical cavities mediate an effective hopping between the phonon modes b_1 and b_2, where the overall phase is controlled by the phases $\phi_{1,2}$ of the external driving fields. (c) Scattering probabilities $|\mathcal{S}_{1\to j}(\omega)|^2$ into the different ports $j=1,2,3$ of the circulator for an incoming signal of frequency ω in port 1. The solid line shows the results for an ideal device ($\gamma_0=0$) and the dashed lines the results for a finite intrinsic loss rate $\gamma_0=\gamma/20$ for each of the three local phonon modes.

Including the coupling to the waveguides and in a frame rotating with the resonator frequencies $\omega_{\rm m}$, the QLEs read

$$\begin{pmatrix}\dot{b}_1\\ \dot{b}_2\\ \dot{b}_3\end{pmatrix}=-\begin{pmatrix}\gamma/2 & \mathrm{i}t\,\mathrm{e}^{-\mathrm{i}\varphi} & \mathrm{i}t\\ \mathrm{i}t\,\mathrm{e}^{\mathrm{i}\varphi} & \gamma/2 & \mathrm{i}t\\ \mathrm{i}t & \mathrm{i}t & \gamma/2\end{pmatrix}\begin{pmatrix}b_1\\ b_2\\ b_3\end{pmatrix}-\sqrt{\gamma}\begin{pmatrix}b_{1,\rm in}\\ b_{2,\rm in}\\ b_{3,\rm in}\end{pmatrix}, \tag{55}$$

with the input–output relations $b_{j,\rm out}=b_{j,\rm in}+\sqrt{\gamma}b_j$. The above set of QLEs can be solved in Fourier space and the input relation can be applied to obtain the full scattering matrix $\mathcal{S}(\omega)$ of this system. By choosing $\varphi=\pi/2$ and $t=\gamma/2$, such that the decays into the waveguides match the tunneling amplitudes, we find that for frequencies around $\omega\simeq\omega_{\rm m}$ ($\omega\simeq 0$ in the rotating frame), the scattering matrix is given by

$$\begin{pmatrix}b_{1,\rm out}\\ b_{2,\rm out}\\ b_{3,\rm out}\end{pmatrix}=\begin{pmatrix}0 & 1 & 0\\ 0 & 0 & \mathrm{i}\\ \mathrm{i} & 0 & 0\end{pmatrix}\begin{pmatrix}b_{1,\rm in}\\ b_{2,\rm in}\\ b_{3,\rm in}\end{pmatrix}. \tag{56}$$

Up to factors i, which can be absorbed in the definitions of the operators, equation (56) describes a perfect circulator. For $\varphi = -\pi/2$ we obtain a similar result, but with the scattering direction reversed, i.e. $b_{1,\mathrm{out}} = \mathrm{i}\, b_{3,\mathrm{in}}$, $b_{2,\mathrm{out}} = b_{1,\mathrm{in}}$ and $b_{3,\mathrm{out}} = \mathrm{i}\, b_{2,\mathrm{in}}$. In figure 8(c) we plot the scattering probabilities $|\mathcal{S}_{1\to j}(\omega)|^2$, defined as $b_{j,\mathrm{out}}(\omega) = \mathcal{S}_{1\to j}(\omega) b_{1,\mathrm{in}}(\omega)$, as a function of the frequency ω (relative to ω_m) and for $t = \gamma/2$. We see the emergence of the ideal circulator relations close to resonance. We also find that these features are robust when we add an additional intrinsic loss rate $\gamma_0 = \gamma/20$.

5.2. Optomechanically engineered non-reciprocity for phonons

To implement a complex tunnel amplitude $t\mathrm{e}^{\mathrm{i}\varphi}$ between two localized mechanical modes, we propose a setup as shown in figure 8(b). Here, the localized phonon mode b_3 is coupled to modes b_1 and b_2 mechanically with a (real) tunneling amplitude t, while the tunneling between b_1 and b_2 is mediated by two driven optical cavities. The Hamiltonian for this system is

$$H_\mathrm{circ} = \sum_{i=1}^{3} \omega_\mathrm{m} b_i^\dagger b_i + t\,(b_1 b_3^\dagger + b_2 b_3^\dagger + \mathrm{H.c.}) + H_\mathrm{c} + H_\mathrm{om}. \tag{57}$$

In the frame rotating with the frequency of an external driving field, the Hamiltonian for the two coupled optical cavities is

$$H_\mathrm{c} = -\sum_{i=1,2} \delta_i a_i^\dagger a_i - J(a_1 a_2^\dagger + a_1^\dagger a_2) + \mathrm{i} \sum_{i=1,2} \mathcal{E}_i \left(a_i^\dagger \mathrm{e}^{\mathrm{i}\phi_i} - \mathrm{H.c.} \right), \tag{58}$$

where $\mathcal{E}_i$ are the strengths and ϕ_i the phases of the optical driving fields. Finally,

$$H_\mathrm{om} = \sum_{i=1,2} g a_i^\dagger a_i (b_i + b_i^\dagger) \tag{59}$$

describes the local OM interactions.

As discussed in section 3, in the limit of strong driving we can change to a displaced representation and linearize the OM coupling around the classical expectation values $\alpha_i = \langle a_i \rangle$. In the present case, the classical field amplitudes are given by

$$\alpha_1 = \frac{(\kappa - \mathrm{i}\delta_2)\mathcal{E}_1 \mathrm{e}^{\mathrm{i}\phi_1} + \mathrm{i}J\mathcal{E}_2 \mathrm{e}^{\mathrm{i}\phi_2}}{(\kappa - \mathrm{i}\delta_1)(\kappa - \mathrm{i}\delta_2) + J^2}, \tag{60}$$

$$\alpha_2 = \frac{(\kappa - \mathrm{i}\delta_1)\mathcal{E}_2 \mathrm{e}^{\mathrm{i}\phi_2} + \mathrm{i}J\mathcal{E}_1 \mathrm{e}^{\mathrm{i}\phi_1}}{(\kappa - \mathrm{i}\delta_1)(\kappa - \mathrm{i}\delta_2) + J^2}, \tag{61}$$

where we have assumed that both cavities decay with the same rate κ and we have absorbed nonlinear shifts of the detunings by a redefinition of δ_i. We write $\alpha_i = |\alpha_i| \mathrm{e}^{\mathrm{i}\varphi_i}$ and obtain the linearized OM coupling

$$H_\mathrm{om} = \sum_{i=1,2} g|\alpha_i| (\mathrm{e}^{-\mathrm{i}\varphi_i} a_i + \mathrm{e}^{\mathrm{i}\varphi_i} a_i^\dagger)(b_i + b_i^\dagger). \tag{62}$$

Note that for given δ_i, J and κ the external control parameters $\mathcal{E}_i$ and ϕ_i provide enough flexibility to independently adjust the phases φ_i and keep $|\alpha_1| \approx |\alpha_2|$.

We focus on the specific case $\delta_i = \delta$, $|\alpha_i| = \alpha$ and introduce symmetric and anti-symmetric optical modes $a_\pm = (a_1 \pm a_2)/\sqrt{2}$ with detunings $\delta_\pm = \delta \pm J$. Further, we assume that

$-\delta_\pm \approx \omega_\mathrm{m} \gg g|\alpha_i|$, which allows us to make a RWA with respect to ω_m. Then, after changing to a frame rotating with ω_m, the total Hamiltonian is given by

$$H_\mathrm{circ} = -\sum_{\nu=\pm} \Delta_\nu a_\nu^\dagger a_\nu + t(b_1 b_3^\dagger + b_2 b_3^\dagger + \mathrm{H.c.}) + \frac{g\alpha}{\sqrt{2}}[a_+^\dagger(\mathrm{e}^{\mathrm{i}\varphi_1} b_1 + \mathrm{e}^{\mathrm{i}\varphi_2} b_2) + a_-^\dagger(\mathrm{e}^{\mathrm{i}\varphi_1} b_1 - \mathrm{e}^{\mathrm{i}\varphi_2} b_2) + \mathrm{H.c.}], \tag{63}$$

where $\Delta_\nu = \delta_\nu + \omega_\mathrm{m}$. In a final step we assume that $|\Delta_\nu| \gg g\alpha$ and treat the OM coupling using second-order perturbation theory. Apart from small frequency shifts for the mechanical modes this results in an effective tunneling Hamiltonian

$$H_\mathrm{circ} \simeq t b_1 b_3^\dagger + t b_2 b_3^\dagger + t_\mathrm{eff} \mathrm{e}^{\mathrm{i}\varphi} b_1 b_2^\dagger + \mathrm{H.c.}, \tag{64}$$

where $\varphi = \varphi_1 - \varphi_2$ and

$$t_\mathrm{eff} = \frac{g^2\alpha^2}{2}\left(\frac{1}{\Delta_+} - \frac{1}{\Delta_-}\right). \tag{65}$$

Thus, by choosing the external control parameters such that $\varphi = \pm\pi/2$ and that t_eff matches the bare mechanical tunneling amplitude t, the setup shown in figure 8(b) realizes a switchable three-port phonon circulator, as discussed in the previous subsection. Note that the interaction with the optical modes also introduces an additional decay channel with rate $\gamma_\mathrm{op} \approx g^2\alpha^2\kappa/\bar{\Delta}^2$, where $\bar{\Delta}^{-2} = \Delta_+^{-2} + \Delta_-^{-2}$. Compared to the noise filtering scheme described above, this requires slightly lower cavity decays satisfying $\kappa \ll |\bar{\Delta}| \ll \omega_\mathrm{m}$.

As a specific example let us consider the phonon waveguide scenario discussed above with typical phonon frequencies $\omega_\mathrm{m} \approx 2\pi \times 4\,\mathrm{GHz}$ and a phonon–waveguide coupling of $\gamma = 2\pi \times 25\,\mathrm{MHz}$. If we choose $\delta_i = -\omega_\mathrm{m}$ we obtain $t_\mathrm{eff} = g^2\alpha^2/J$ and the conditions $t_\mathrm{eff} = \gamma/2$ can be achieved for $g\alpha \approx 2\pi \times 110\,\mathrm{MHz}$ and $J = 2\pi \times 1\,\mathrm{GHz}$. For the same parameters a value of $\kappa \leqslant 2\pi \times 50\,\mathrm{MHz}$ is sufficient to suppress the optically induced decay rate $\gamma_\mathrm{op} = 2\,g^2\alpha^2\kappa/J^2$ below the value $\gamma_\mathrm{op}/\gamma \leqslant 0.05$ shown in figure 8(c). This is only slightly below the demonstrated values for κ in state-of-the-art OM crystal cavities [22, 25].

6. Implementations

The fabrication and control of mechanical systems, resonator arrays and phonon waveguides as well as their coupling to other microscopic quantum systems (qubits) is currently a very active field of research. For many of these systems the general control techniques described in this paper could provide the basis for phonon-based quantum communication applications or mechanical quantum interfaces in hybrid qubit setups. In the following, we present a brief discussion of several potential candidate systems for implementing phonon networks.

6.1. Phonon channels

As described in section 2, a 1D phonon channel can be realized by fabricating a large array of coupled nanomechanical resonators with a bare frequency ω_m and nearest-neighbor coupling $K < \omega_\mathrm{m}$. This scenario has been experimentally studied, for example in [37], where the resonators were charged up and coupled via electrostatic interactions. Alternatively, the resonators can also be coupled mechanically via bridges or the support [46]. Both approaches are suitable for realizing phonon channels with frequencies ω_m ranging from MHz to a few

hundreds of MHz, where also very high Q-values around $Q \sim 10^5$–10^6 are now routinely achieved. At $T \approx 100\,\mathrm{mK}$ this frequency range corresponds to a few tens to a few hundreds of thermal phonons, which can still be efficiently suppressed using the proposed OM noise filtering scheme.

A more practical and very versatile approach for implementing phonon waveguides based on phononic bandgap materials has in recent years attracted increasing attention [32, 33]. Here, a 2D structure with periodically varying mechanical properties is designed such that a complete band gap in the mechanical dispersion relation appears. Then, phonon wave guides can be realized by introducing line defects into these structures, to which the phonons are confined as long as their frequency lies within the bandgap of the bulk phononic crystal. With this approach phonon waveguides with frequencies $\omega_\mathrm{m} \approx 1$–$10\,\mathrm{GHz}$ can be realized, where even at $T = 4\,\mathrm{K}$ the thermal occupation of the waveguide is only a few tens of quanta. Further, as indicated in figure 1(b), such waveguides can be easily combined with localized phonon cavities and integrated OM devices [25].

6.2. *Qubit–phonon interfaces*

The implementation of phonon quantum networks also requires the realization of coherent and controllable interfaces between mechanics and stationary qubits. Here the ability of mechanical systems to respond to weak optical, electrical and magnetic forces enables the coupling of mechanical resonators to a wide variety of spin- or charge-based qubits and a few prototype examples are outlined in the following.

6.2.1. Spin qubits. Qubits encoded in localized spin degrees of freedom, for example in spins associated with nitrogen vacancy (NV) impurities in diamond [47] or phosphor donors in silicon [48], can be coupled to mechanical motion using magnetized tips [13, 14, 49]. A strong magnetic field gradient ∇B from the tip induces a position-dependent Zeeman shift of the spin, resulting in an interaction of the form

$$H_\mathrm{node} = \frac{\omega_0}{2}\sigma_z + \omega_\mathrm{m} b^\dagger b + \lambda(b + b^\dagger)\sigma_z + \frac{\Omega}{2}\cos(\omega_\mathrm{mw} t)\sigma_x. \tag{66}$$

Here $\omega_0 \sim$ GHz is the bare spin splitting and $\lambda = g_s \mu_\mathrm{B} a_0 \nabla B/(2\hbar)$ is the Zeeman shift per zero point motion a_0, where $g_s \simeq 2$ and μ_B is the Bohr magneton. For nano-scale mechanical resonators with frequencies in the few MHz regime, this coupling can be substantial and reach values $\lambda/(2\pi) \approx 10$–$100\,\mathrm{kHz}$ [50]. Based on this coupling the use of mechanical transducers to mediate spin–spin interactions in small resonator arrays has been proposed previously [23], and the present techniques can be used to extend these ideas to larger networks. To achieve an effective Jaynes–Cummings-type interaction as given in equation (2), the spin is driven by a near-resonant microwave field with frequency $\omega_\mathrm{mw} = \omega_0 + \delta$ and Rabi frequency Ω as described by the last term in equation (66). Then, by changing into a dressed spin basis and making an RWA with respect to ω_0, the effective interaction is given as [43, 50]

$$H_\mathrm{node} \simeq \frac{\Delta_\mathrm{q}}{2}\tilde{\sigma}_z + \omega_\mathrm{m} b^\dagger b + \lambda \sin(\theta)(\tilde{\sigma}_+ b + \tilde{\sigma}_- b^\dagger), \tag{67}$$

where $\Delta_\mathrm{q} = \sqrt{\delta^2 + \Omega^2} \sim \omega_\mathrm{m}$ and $\tan(\theta) = \Omega/\delta$. The qubit–resonator coupling can be controlled by adiabatically varying the effective detuning Δ_q or the mixing angle θ.

Instead of using external magnetic field gradients, alternative schemes to strongly couple spins to mechanical motion have recently been suggested for carbon nanotubes [51, 52]. Here a single electron is localized on the nanotube and couples to its vibration via spin–orbit interactions. In this case even larger couplings $\lambda/(2\pi) \approx 0.5\,\mathrm{MHz}$ and larger mechanical frequencies $>100\,\mathrm{MHz}$ are achievable. Although a controlled fabrication and positioning of carbon nanotubes is still challenging, a phonon quantum bus could be realized by electrically coupling the nanotube to other mechanical resonators, which can be fabricated in a more controlled manner.

6.2.2. Superconducting qubits. The coupling of nanomechanical systems to various types of superconducting qubits has been demonstrated in recent experiments [9, 12, 53]. While for superconducting qubits other ways for communication exist, for example via microwave transmission lines, the coupling to phononic channels could still be interesting for creating interfaces to other quantum systems, especially to optical qubits for long-distance quantum communication [24, 25]. Depending on the type of qubit ('charge', 'phase', 'flux', etc) the qubit–resonator interaction can be due to electrostatic [17, 54], piezo-electric [9] or magnetic interactions [55–57], and can in all three cases be substantially larger than in the case of spin qubits. Since the bare transition frequency of superconducting qubits is typically in the GHz regime, a resonant coupling to mechanical systems in the MHz range can again be achieved as described above, namely by applying additional driving fields to compensate for the frequency mismatch [54, 58]. Alternatively, superconducting qubits could be coupled directly to high-frequency mechanical modes as demonstrated in [9].

6.2.3. Quantum dots and defect centers. The bending of a mechanical resonator locally deforms the lattice configuration of the host material and by that shifts the electronic states associated with artificial quantum dots or naturally occurring defect centers in solids. In the bulk this deformation potential interaction is usually responsible for the line broadening of optical transitions and other decoherence effects, but in the case of confined modes it can also lead to a significant coherent coupling to single phonons. In [59] the coupling of a quantum dot to the fundamental bending mode of a doubly clamped beam has been considered, leading to a deformation potential coupling of the form

$$H_{\mathrm{def}} = \lambda(b + b^{\dagger})|e\rangle\langle e|, \quad \hbar\lambda \approx (\Xi_{\mathrm{e}} - \Xi_{\mathrm{g}})\frac{a_0 t}{2l^2}, \tag{68}$$

where $|e\rangle$ denotes the electronically excited state, l is the beam length, t is its thickness and a_0 is the zero point motion. The Ξ_{e} and Ξ_{g} are deformation potential constants for the ground and excited electronic states, and for typical values $\Xi_{\mathrm{e,g}} \sim 1$–$10$ eV and micron-sized beams a coupling strength of $\lambda/2\pi \approx 10\,\mathrm{MHz}$ can be achieved. This is already comparable to the radiative lifetime Γ_{e} of the electronically excited state, but can, in principle, be pushed to values $\lambda \sim 1\,\mathrm{GHz}$ using much smaller, phononic Bragg cavities as suggested in [60].

As a potential scenario where the deformation potential interactions could be used to implement a controllable qubit–phonon interface, we consider an NV center embedded in a diamond nanoresonator. The electronic ground state of the NV defect is a spin triplet, where two states $|0\rangle = |m_s = -1\rangle$ and $|1\rangle = |m_s = 1\rangle$ can be used to encode quantum information. The qubit states in the electronic ground state, which are highly immune against external perturbations, can be coupled via an optical Raman process involving an electronically excited

state, which, in contrast, is strongly coupled to phonons [61]. In appendix D we adiabatically eliminate the dynamics of the excited state and derive an effective spin–phonon interaction of the form

$$H_{\rm eff} \simeq \lambda_{\rm eff}(t)(\sigma_+ b + \sigma_- b^\dagger). \tag{69}$$

Here the $\sigma_\pm$ are Pauli operators for the qubit subspace and for optimized laser detunings $\lambda_{\rm eff}(t) = 4\lambda\Omega_0(t)\Omega_1(t)/\omega_{\rm m}^2$ is a tunable coupling where $\Omega_{0,1}(t)$ are the optical Rabi frequencies. Note that this coherent interaction is accompanied by dissipation at an average rate $\bar{\Gamma}_{\rm eff}(t) = 4\lambda\Omega_0(t)\Omega_1(t)/\omega_{\rm m}^2$ and the ratio $\lambda_{\rm eff}/\bar{\Gamma}_{\rm eff} = \lambda/\Gamma$ is not affected by the off-resonant Raman coupling. This is in contrast to cavity QED where the optical field couples to the atomic coherence and not to the population of the excited state as described by $H_{\rm def}$.

7. Conclusions and outlook

In summary, we have described the implementation of dissipative as well as coherent OM control elements for realizing quantum communication protocols in extended phononic networks. We have shown how OM continuous mode cooling schemes can be used to create a cold frequency window in the thermal noise spectrum of a phononic channel and we have analyzed the fidelity of quantum state-transfer protocols under these conditions. Further, we have proposed the realization of non-reciprocal phononic elements, which rely on strong coherent OM interactions and where the directionality is simply controlled by the phase of an external laser field. Based on this principle, various switches and routers for propagating phonons can be constructed, which also allow for the implementation of efficient quantum communication protocols in larger phonon networks.

Both the OM noise filter and the phonon router can be realized with state-of-the-art mechanical systems. Combined with the ongoing developments in the control of qubit–resonator interactions, they could soon provide the elemental tools for implementing phononic quantum networks. As potential applications of such networks we envision the distribution of entanglement within a larger quantum computing architecture, where propagating phonons can replace or complement direct qubit shuttling techniques [62, 63]. Here the ability of mechanical systems to interact with various different types of qubits makes phononic channels particularly suited for hybrid qubit settings. Beyond quantum communication applications, the OM control techniques described here may also be used to probe the propagation and scattering of single-phonon wave packets.

Acknowledgments

The authors thank S Bennett, F Marquardt, O Painter and A Safavi-Naeini for stimulating discussions. This work was supported by the EU network AQUTE and the Austrian Science Fund (FWF) through SFB FOQUS and the START grant Y 591-N16. ML acknowledges support from NSF, CUA, DARPA and the Packard Foundation.

Appendix A. Coupled resonator arrays

In this appendix, we derive the effective propagation equations and input–output relations for phononic quantum channels consisting of a large array of $N_{\rm ch} \gg 1$ coupled mechanical

resonators. Assuming a homogenous system the resonator array is described by the Hamiltonian

$$H_{\text{channel}} = \sum_{\ell=1}^{N_{\text{ch}}} \left(\frac{p_\ell^2}{2m} + \frac{1}{2} m\omega_0^2 x_\ell^2 \right) + \frac{k}{2} \sum_{\ell=1}^{N_{\text{ch}}-1} (x_\ell - x_{\ell+1})^2, \tag{A.1}$$

and the equations of motion for the position operators x_ℓ are given by

$$\ddot{x}_\ell = -\omega_0^2 x_\ell - \omega_0 K (2x_\ell - x_{\ell+1} - x_{\ell-1}), \tag{A.2}$$

where $K = k/(m\omega_0)$ is the nearest-neighbor phonon–phonon coupling strength. For a large array, we can assume periodic boundary conditions and write

$$x_\ell(t) = \frac{1}{\sqrt{N_{\text{ch}}}} \sum_n \sqrt{\frac{\hbar}{2m\omega_n}} \left(\mathrm{e}^{\mathrm{i}2\pi n\ell/N_{\text{ch}}} b_n(t) + \mathrm{e}^{-\mathrm{i}2\pi n\ell/N_{\text{ch}}} b_n^\dagger(t) \right), \tag{A.3}$$

where $b_n(t) = b_n \mathrm{e}^{-i\omega_n t}$ are bosonic operators for the plane wave modes labeled by $n = -(N_{\text{ch}}/2 - 1), \ldots, N_{\text{ch}}/2$ and normalized to $[b_n, b_{n'}^\dagger] = \delta_{n,n'}$. The eigenfrequencies are given by

$$\omega_n = \sqrt{\omega_0^2 + 2K\omega_0 [1 - \cos(2\pi n/N_{\text{ch}})]}. \tag{A.4}$$

We are interested in the regime where the total length L as well as the other relevant scales of the network are large compared to the spacing a between the individual resonators. We introduce a continuous field

$$\Xi(z) = \frac{1}{\sqrt{N_{\text{ch}}}} \sum_q \sqrt{\frac{\hbar}{2m\omega_q}} \left(\mathrm{e}^{\mathrm{i}qz} b_q + \mathrm{e}^{-\mathrm{i}kz} b_k^\dagger \right), \tag{A.5}$$

such that $x_\ell = \Xi(z = a\ell)$. The quasi-momentum q is restricted to the first Brillouin zone $q \in (-\pi/a, \pi/a]$ and $\omega_q = \sqrt{\omega_0^2 + 2K\omega_0 [1 - \cos(qa)]}$.

To proceed we now consider the tight binding limit $K \ll \omega_0$, where $\omega_q \simeq \omega_0 + K(1 - \cos(qa))$ and the phonon modes form a band of width $\Delta\omega = 2K$ around a large center frequency $\bar{\omega} = \omega_0 + K$. Further, for frequencies around $\bar{\omega}$ the dispersion relation is approximately linear and can be written as

$$\omega_q \simeq \bar{\omega} + c(|q| - \pi/(2a)) = \tilde{\omega}_0 + c|q|, \tag{A.6}$$

where $c = Ka$ is the sound velocity and $\tilde{\omega}_0 = \omega_0 - (\pi/2 - 1)K$ a frequency offset. Therefore, as long as we are interested in the dynamics of phonon modes away from the band edges, we can set $H_{\text{channel}} \simeq \sum_q (\tilde{\omega}_0 + c|q|) b_q^\dagger b_q$ and approximate the displacement field by

$$\Xi(z) \simeq \frac{\bar{x}_0}{\sqrt{\Delta\omega}} [\Phi(z) + \Phi^\dagger(z)]. \tag{A.7}$$

Here $\bar{x}_0 = \sqrt{\hbar/2m\bar{\omega}}$ and the field $\Phi(z) = \sqrt{2c/L} \sum_q \mathrm{e}^{\mathrm{i}qz} b_q$ is normalized to

$$\left[\Phi(z, t), \Phi^\dagger(z', t') \right] \simeq \mathrm{e}^{-\mathrm{i}\tilde{\omega}_0(t-t')} \left[\delta\left(\Delta t - \frac{\Delta z}{c} \right) + \delta\left(\Delta t + \frac{\Delta z}{c} \right) \right], \tag{A.8}$$

where $\Delta t = t - t'$ and $\Delta z = z - z'$. The field operators can be decomposed into a right- and a left-moving component $\Phi(z) = \Phi_{\rm R}(z) + \Phi_{\rm L}(z)$, as defined in equations (4) and (5).

The coupling of the localized phonon modes to the phonon channel can be written as

$$H_{\rm int} = \frac{1}{2}\sum_{i=1}^{N}\sum_{\ell} k_{i,\ell}(x_i - x_\ell)^2, \tag{A.9}$$

where $k_{i,\ell} = k_{\rm loc}$ is non-zero only for site ℓ, which are next to a local mode i (we can assume side-coupled resonators, such that there is only one neighbor). We define $K_{\rm loc} = k_{\rm loc} x_0 \bar{x}_0$ where x_0 is the zero point motion of the local mode. Then, under the assumption that $\omega_{\rm m} \approx \bar{\omega} \gg K_{\rm loc}$, we can make an RWA and obtain the coupling given in equation (6) with a resonator decay rate given by $\gamma = 2K_{\rm loc}^2/\Delta\omega$.

A.1. Propagation losses

To model propagation losses in the phonon waveguide we add an intrinsic loss channel with rate γ_0 for each of the waveguide modes. Making the RWA right from the beginning, the dynamics of the whole resonator array is modeled by the coupled QLEs,

$$\dot{b}_\ell = -\left(\mathrm{i}(\omega_0 + K) + \frac{\gamma_0}{2}\right) b_\ell + \frac{\mathrm{i}K}{2}\,(b_{\ell-1} + b_{\ell+1}) - \sqrt{\gamma_0}\, b_{\ell,\rm in}(t), \tag{A.10}$$

where b_ℓ is the bosonic operator for the mechanical resonator at site ℓ and the $b_{\ell,\rm in}(t)$ are uncorrelated thermal noise operators $\langle b^\dagger_{\ell,\rm in}(t) b_{\ell',\rm in}(t')\rangle = N_{\rm th}\delta_{\ell,\ell'}\delta(t-t')$. In the corresponding momentum representation $b_q = 1/\sqrt{N_{\rm ch}}\sum_\ell \mathrm{e}^{\mathrm{i}qa\ell} b_\ell$ and $b_{q,\rm in} = 1/\sqrt{N_{\rm ch}}\sum_\ell \mathrm{e}^{\mathrm{i}qa\ell} b_{\ell,\rm in}$, the coupling is diagonal

$$\dot{b}_q = -\left(\mathrm{i}\,\omega_q + \frac{\gamma_0}{2}\right) b_q - \sqrt{\gamma_0}\, b_{q,\rm in}(t), \tag{A.11}$$

where as above $\omega_q = \omega_0 + K(1 - \cos(qa)) \approx \tilde{\omega}_0 + c|q|$. From this equation we obtain the propagation equation for the right-moving field $\Phi_{\rm R}(z,t) = \sqrt{2c/L}\sum_{q>0}\mathrm{e}^{\mathrm{i}qz} b_q(t)$,

$$\left(\frac{\partial}{\partial t} + c\frac{\partial}{\partial z}\right)\Phi_{\rm R}(z,t) = -\left(\mathrm{i}\tilde{\omega}_0 + \frac{\gamma_0}{2}\right)\Phi_{\rm R}(z,t) - \sqrt{\gamma_0 c}\,\Phi_{\rm th}(z,t). \tag{A.12}$$

Here the thermal noise field is defined as

$$\Phi_{\rm th}(z,t) = \sqrt{\frac{2}{L}}\sum_{q>0}\mathrm{e}^{\mathrm{i}qz} b_{q,\rm in}(t), \tag{A.13}$$

such that it is normalized as $\langle \Phi^\dagger_{\rm th}(z,t)\Phi_{\rm th}(z',t')\rangle = N_{\rm th}\delta(z-z')\delta(t-t')$.

Appendix B. Optomechanical cooling

After linearizing the OM coupling the QLEs (13) and (14) can be written as

$$\partial_t \vec{A}(t) = -\mathcal{M}\vec{A}(t) - \sqrt{2\kappa}\,\vec{A}_{\rm in}(t) - \sqrt{\gamma_0}\,\vec{B}_{0,\rm in}(t), \tag{B.1}$$

where we have grouped operators as $\vec{A}(t) = (a(t), a^\dagger(t), b(t), b^\dagger(t))^{\mathrm{T}}$, $\vec{A}_{\mathrm{in}}(t) = (a_{\mathrm{in}}(t), a^\dagger_{\mathrm{in}}(t), 0, 0)^{\mathrm{T}}$ and $\vec{B}_{0,\mathrm{in}}(t) = (0, 0, b_{0,\mathrm{in}}(t), b^\dagger_{0,\mathrm{in}}(t))^{\mathrm{T}}$. The matrix $\mathcal{M}$ is given by

$$\mathcal{M} = \begin{pmatrix} -\mathrm{i}\delta + \kappa & 0 & \mathrm{i}g\alpha & \mathrm{i}g\alpha \\ 0 & \mathrm{i}\delta + \kappa & -\mathrm{i}g\alpha^* & -\mathrm{i}g\alpha^* \\ \mathrm{i}g\alpha^* & \mathrm{i}g\alpha & \mathrm{i}\omega_{\mathrm{m}} + \frac{\gamma_0}{2} & 0 \\ -\mathrm{i}g\alpha & -\mathrm{i}g\alpha^* & 0 & -\mathrm{i}\omega_{\mathrm{m}} + \frac{\gamma_0}{2} \end{pmatrix}. \tag{B.2}$$

We define the Fourier-transformed operators as $a(\omega) = \frac{1}{\sqrt{2\pi}} \int \mathrm{d}t\ \mathrm{e}^{\mathrm{i}\omega t} a(t)$, $a^\dagger(\omega) = [a(\omega)]^\dagger$ and obtain

$$\vec{A}(\omega) = -\mathcal{X}(\omega)\left(\sqrt{2\kappa}\,\vec{A}_{\mathrm{in}}(\omega) + \sqrt{\gamma_0}\vec{B}_{0,\mathrm{in}}(\omega)\right), \tag{B.3}$$

where we set $\mathcal{X}(\omega) = [\mathcal{M} - \mathrm{i}\,\omega\mathbb{1}]^{-1}$ and now $\vec{A}(\omega) = (a(\omega), a^\dagger(-\omega), b(\omega), b^\dagger(-\omega))^{\mathrm{T}}$, etc. The non-vanishing correlations of the noise operators are $\langle a_{\mathrm{in}}(\omega) a^\dagger_{\mathrm{in}}(\omega')\rangle = \delta(\omega - \omega')$, $\langle b_{0,\mathrm{in}}(\omega) b^\dagger_{0,\mathrm{in}}(\omega')\rangle = (N_{\mathrm{th}} + 1)\delta(\omega - \omega')$ and $\langle b^\dagger_{0,\mathrm{in}}(\omega) b_{0,\mathrm{in}}(\omega')\rangle = N_{\mathrm{th}}\delta(\omega - \omega')$, within the relevant frequency range. Then, the stationary fluctuation spectrum of the mechanical mode is given by

$$\langle b^\dagger(\omega) b(\omega')\rangle = [2\kappa|\mathcal{X}(\omega)_{32}|^2 + \gamma_0 N_{\mathrm{th}}(|\mathcal{X}(\omega)_{33}|^2 + |\mathcal{X}(\omega)_{34}|^2)]\delta(\omega - \omega'). \tag{B.4}$$

Under the weak coupling and sideband resolved condition this expression simplifies to the result given in equation (17).

In section 3.3, we are interested in a spectrum of the scattered field $b_{\mathrm{out}}(t)$ in the case in which the OMS is in addition coupled to the phonon waveguide with rate γ. We define $\vec{A}(\omega)$ and the intrinsic noise $\vec{B}_{0,\mathrm{in}}(\omega)$ as above, but we set $\vec{A}_{\nu=\mathrm{in,out}}(\omega) = (a_\nu(\omega), a^\dagger_\nu(-\omega), b_\nu(\omega), b^\dagger_\nu(-\omega))^{\mathrm{T}}$. The input–output relations can then be written as $\vec{A}_{\mathrm{out}}(\omega) = \vec{A}_{\mathrm{in}}(\omega) + \sqrt{\mathcal{R}}\vec{A}(\omega)$ where $\mathcal{R} = \mathrm{diag}(2\kappa, 2\kappa, \gamma, \gamma)$ is a diagonal matrix. Then, together with equation (B.3) we obtain

$$\vec{A}_{\mathrm{out}}(\omega) = \mathcal{S}(\omega)\vec{A}_{\mathrm{in}}(\omega) - \mathcal{S}'(\omega)\vec{B}_{0,\mathrm{in}}(\omega), \tag{B.5}$$

where $\mathcal{S}(\omega) = \mathbb{1} - \mathcal{R}\mathcal{X}(\omega)$ and $\mathcal{S}'(\omega) = \sqrt{\gamma_0\mathcal{R}}\mathcal{X}(\omega)$ and in the definition of $\mathcal{X}(\omega)$ we replaced $\gamma_0 \to \gamma_0 + \gamma$. The filtered noise spectrum of the out-field is given by

$$N_{\mathrm{F}}(\omega) = |\mathcal{S}(\omega)_{32}|^2 + N_{\mathrm{th}}(|\mathcal{S}(\omega)_{33}|^2 + |\mathcal{S}(\omega)_{34}|^2 + |\mathcal{S}'(\omega)_{33}|^2 + |\mathcal{S}'(\omega)_{34}|^2), \tag{B.6}$$

where in equation (28) the approximation $N_{\mathrm{F}}(\omega) \simeq N_{\mathrm{th}}|\mathcal{S}(\omega)_{33}|^2$ has been made.

B.1. Multi-mode cooling

We can use the same approach to solve for the stationary state of the multi-mode system described in section 3.2. In the following we assume for simplicity the validity of the RWA, such that the QLEs for the equations for the annihilation operators $\vec{A} = (a, b_1, \ldots b_N)^{\mathrm{T}}$ form a closed set

$$\partial_t \vec{A}(t) = -\mathcal{M}\vec{A}(t) - \sqrt{2\kappa}\,\vec{A}_{\mathrm{in}}(t) - \sqrt{\gamma_0}\vec{B}_{0,\mathrm{in}}(t), \tag{B.7}$$

where now $\vec{A}_{\mathrm{in}}(t) = (a_{\mathrm{in}}(t), 0, \ldots, 0)^{\mathrm{T}}$ and $\vec{B}_{0,\mathrm{in}}(t) = (0, b^{(1)}_{0,\mathrm{in}}(t), \ldots, b^{(N)}_{0,\mathrm{in}}(t))^{\mathrm{T}}$ and the matrix $\mathcal{M}$ can be derived from equations (19)–(22). Following the same steps as above, we obtain

$$\langle b^\dagger_i(\omega) b_i(\omega')\rangle = \gamma_0 N_{\mathrm{th}} \left(\sum_{j=1}^{N} \left|\mathcal{X}(\omega)_{i+1,j+1}\right|^2\right) \delta(\omega - \omega'), \tag{B.8}$$

which we have used for evaluating the multi-mode cooling results presented in figure 4(c).

Appendix C. The cascaded master equation

To simulate the state transfer between two nodes in the presence of incident noise and OM cooling, we map the qubit QLEs (38) and (39) with time-dependent decay rates $\Gamma_1(t)$ and $\Gamma_2(t)$ onto an equivalent cascaded master equation [38], which we can then integrate numerically. Since we cannot treat the filtered input noise directly using a master equation, we consider a unidirectional network where the OM cooled phonon cavity is included as a first system. The OM cooling is modeled by an additional decay channel for the phonon cavity at a rate $\gamma_{\rm op} = 2g^2|\alpha|^2/\kappa$, which matches the decay rate γ of the phonon cavity into the waveguide. The cascaded master equation, which describes this system, is given by

$$\dot{\rho} = -\mathrm{i}[H,\,\rho] + (N_{\rm th}+1)\mathcal{D}[S]\rho + N_{\rm th}\mathcal{D}[S^\dagger]\rho + \gamma_{\rm op}\mathcal{D}[b]\rho, \tag{C.1}$$

where $\mathcal{D}[c]\rho = c\rho c^\dagger - (c^\dagger c\rho + \rho c^\dagger c)/2$. By identifying $c_0 \equiv b$, $c_{j=1,2} = \sigma_-^j$ and $\Gamma_0 = \gamma$ the collective operator $S = \sum_{k=0,1,2}\sqrt{\Gamma_k}c_k$ and $H = -\frac{\mathrm{i}}{2}\sum_{k>l}\sqrt{\Gamma_k\Gamma_l}(c_k^\dagger c_l - c_l^\dagger c_k)$. $N_{\rm th}$ is the thermal occupation number of the incident white noise.

Appendix D. Nitrogen vacancy–phonon coupling

In this appendix, we show how for an NV center in diamond the deformation potential coupling can be used to realize the effective spin–phonon interaction (69). The NV center has an $S = 1$ triplet ground state and we assume that the qubit is encoded in the states $|0\rangle \equiv |m_s = -1\rangle$ and $|1\rangle = |m_s = +1\rangle$. The qubit states are coupled by external laser fields to an electronically excited state $|e\rangle$, which is coupled to the deformation of the local lattice structure induced by the vibration of the beam. In the frame rotating with the laser frequencies the Hamiltonian is given by

$$H = \sum_{j=0,1}[\Delta_j|j\rangle\langle j| + \Omega_j(t)(|j\rangle\langle e| + |e\rangle\langle j|)] + \omega_{\rm m}b^\dagger b + \lambda|e\rangle\langle e|(b+b^\dagger), \tag{D.1}$$

where the $\Omega_j(t)$ are tunable Rabi frequencies and we have chosen the zero of energy to coincide with the excited state level such that Δ_0 and Δ_1 are detunings of the drive lasers from the $|0\rangle$ to $|e\rangle$ and the $|1\rangle$ to $|e\rangle$ transitions, respectively. The interaction term $\sim\lambda$ can be eliminated by a *polaron transformation*

$$H \to \mathrm{e}^S H \mathrm{e}^{-S} \quad \text{with} \quad S = \frac{\lambda}{\omega_{\rm m}}|e\rangle\langle e|(b^\dagger - b), \tag{D.2}$$

which transforms the Hamiltonian into

$$H = \omega_{\rm m}b^\dagger b + \sum_{j=0,1}\Delta_j|j\rangle\langle j| + [(\Omega_0|0\rangle\langle e| + \Omega_1|1\rangle\langle e|)\,A + \mathrm{H.c.}] \tag{D.3}$$

and is still exact. Since the ratio $\eta \equiv \lambda/\omega_{\rm m} \ll 1$, we can expand to first order in η and obtain $A \simeq 1 - \eta(b^\dagger - b)$.

Our goal is to induce a coherent Raman transition from state $|0\rangle$ to state $|1\rangle$ while simultaneously absorbing a phonon from the nanomechanical oscillator. To make this process resonant, we set $\Delta_0 = \Delta + \omega_{\rm m}/2$ and $\Delta_1 = \Delta - \omega_{\rm m}/2$, where $\Delta = (\Delta_0 + \Delta_1)/2$ is the overall detuning. We change into an interaction picture with respect to $H_0 = \omega_{\rm m}b^\dagger b + \sum_{j=0,1}\Delta_j|j\rangle\langle j|$

and write the total state as $|\tilde{\psi}\rangle(t) = \sum_{j=0,1,e} |\tilde{\psi}_j\rangle(t)$. The equations of motion are then given by

$$\partial_t |\tilde{\psi}_e\rangle(t) = -\frac{\Gamma_e}{2}|\tilde{\psi}_e\rangle(t) - \mathrm{i}\sum_{j=0,1} \Omega_j \mathrm{e}^{-\mathrm{i}\Delta_j t}\left(1 + \eta \mathrm{e}^{\mathrm{i}\,\omega_m t} b^\dagger - \eta \mathrm{e}^{-\mathrm{i}\omega_m t} b\right)|\tilde{\psi}_j\rangle(t) \tag{D.4}$$

$$\partial_t |\tilde{\psi}_{j=0,1}\rangle(t) = -\mathrm{i}\Omega_j \mathrm{e}^{\mathrm{i}\Delta_j t}\left(1 - \eta \mathrm{e}^{\mathrm{i}\,\omega_m t} b^\dagger + \eta \mathrm{e}^{-\mathrm{i}\omega_m t} b\right)|\tilde{\psi}_e\rangle(t), \tag{D.5}$$

where we have added an imaginary part to model the radiative decay of the excited state with rate Γ_e.[6] Assuming that $|\Delta_{0,1}| \gg \Omega_{0,1}$, we can approximately integrate the equation of motion for $|\tilde{\psi}_e\rangle(t)$,

$$|\tilde{\psi}_e\rangle(t) \simeq \sum_{j=0,1} \Omega_j \left(\frac{\mathrm{e}^{-\mathrm{i}\Delta_j t}}{\Delta_j + \mathrm{i}\frac{\Gamma_e}{2}} - \frac{\eta b \mathrm{e}^{-\mathrm{i}(\Delta_j+\omega_m)t}}{(\Delta_j+\omega_m) + \mathrm{i}\frac{\Gamma_e}{2}} + \frac{\eta b^\dagger \mathrm{e}^{-\mathrm{i}(\Delta_j-\omega_m)t}}{(\Delta_j+\omega_m) + \mathrm{i}\frac{\Gamma_e}{2}}\right)|\tilde{\psi}_j\rangle(t), \tag{D.6}$$

and insert this result back into the equations of motion for $|\tilde{\psi}_{0,1}\rangle(t)$. By keeping only non-rotating terms, we obtain for the $|\tilde{\psi}_0\rangle$ subspace,

$$\partial_t |\tilde{\psi}_0\rangle(t) = -\frac{\mathrm{i}\Omega_0^2}{\Delta_0 + \mathrm{i}\frac{\Gamma_e}{2}}|\tilde{\psi}_0\rangle(t) - \mathrm{i}\left[\frac{\eta\Omega_0\Omega_1}{\Delta_1 + \mathrm{i}\frac{\Gamma_e}{2}} - \frac{\eta\Omega_0\Omega_1}{(\Delta_1+\omega_m) + \mathrm{i}\frac{\Gamma_e}{2}}\right] b|\tilde{\psi}_1\rangle(t), \tag{D.7}$$

and a similar result for the evolution of $|\tilde{\psi}_1\rangle(t)$. In the limit $|\Delta_j|, |\Delta_j \pm \omega_m| \gg \Gamma_e$ and using the definition $\Delta_{0,1} = \Delta \pm \omega_m/2$, we can identify an effective spin–phonon coupling λ_{eff} and effective decay rates $\Gamma_{\mathrm{eff}}^{(j)}$ for each spin level,

$$\lambda_{\mathrm{eff}} = \frac{\lambda\Omega_0\Omega_1}{\Delta^2 - \omega_m^2/4}, \quad \Gamma_{\mathrm{eff}}^{(j)} = \Gamma_e \frac{\Omega_j^2}{\Delta_j^2}. \tag{D.8}$$

The ratio between the coherent coupling and the mean decay rate $\bar{\Gamma}_{\mathrm{eff}} = (\Gamma_{\mathrm{eff}}^{(0)} + \Gamma_{\mathrm{eff}}^{(1)})/2$ is optimized for $\Delta = 0$ where $\lambda_{\mathrm{eff}}/\bar{\Gamma}_{\mathrm{eff}} = \lambda/\Gamma_e$.

Here we have assumed that the NV center is coupled to a single vibrational mode. In general, nanostructured resonators will support multiple mechanical modes so that the phononic part in the Hamiltonian (D.1) generalizes to $H_{\mathrm{phonon}} = \sum_k \omega_k (b)_k^\dagger b_k + |e\rangle\langle e| \sum_k \lambda_k (b_k + b_k^\dagger)$. However, since the higher-frequency modes of nanostructured resonators are separated from the fundamental mode by ~GHz, the other modes are highly off-resonant and their contributions to the resulting spin–phonon coupling are negligibly small. See [59] for a similar discussion.

References

[1] Höhberger Metzger C and Karrai K 2004 Cavity cooling of a microlever *Nature* **432** 1002–5
[2] Gigan S, Böhm H R, Paternostro M, Blaser F, Langer G, Hertzberg J B, Schwab K C, Bäuerle D, Aspelmeyer M and Zeilinger A 2006 Self-cooling of a micromirror by radiation pressure *Nature* **444** 67–70
[3] Arcizet O, Cohadon P-F, Briant T, Pinard M and Heidmann A 2006 Radiation-pressure cooling and optomechanical instability of a micromirror *Nature* **444** 71–4
[4] Kleckner D and Bouwmeester D 2006 Sub-kelvin optical cooling of a micromechanical resonator *Nature* **444** 75–8

[6] For simplicity, we omit here the associated recycling terms, which can be included, for example, using a stochastic wave function formalism [38].

[5] Corbitt T, Wipf C, Bodiya T, Ottaway D, Sigg D, Smith N, Whitcomb S and Mavalvala N 2007 Optical dilution and feedback cooling of a gram-scale oscillator to 6.9 mK *Phys. Rev. Lett.* **99** 160801
[6] Thompson J D, Zwickl B M, Jayich A M, Marquardt F, Girvin S M and Harris J G E 2008 Strong dispersive coupling of a high-finesse cavity to a micromechanical membrane *Nature* **452** 72–5
[7] Schliesser A, Rivière R, Anetsberger G, Arcizet O and Kippenberg T J 2008 Resolved-sideband cooling of a micromechanical oscillator *Nature Phys.* **4** 415–9
[8] Wilson D J, Regal C A, Papp S B and Kimble H J 2009 Cavity optomechanics with stoichiometric SiN films *Phys. Rev. Lett.* **103** 207204
[9] O'Connell A D *et al* 2010 Quantum ground state and single-phonon control of a mechanical resonator *Nature* **464** 697–703
[10] Teufel J D, Donner T, Li D, Harlow J W, Allman M S, Cicak K, Sirois A J, Whittaker J D, Lehnert K W and Simmonds R W 2011 Sideband cooling of micromechanical motion to the quantum ground state *Nature* **475** 359–63
[11] Chan J, Mayer Alegre T P, Safavi-Naeini A H, Hill J T, Krause A, Gröblacher S, Aspelmeyer M and Painter O 2011 Laser cooling of a nanomechanical oscillator into its quantum ground state *Nature* **478** 89–92
[12] LaHaye M D, Suh J, Echternach P M, Schwab K C and Roukes M L 2009 Nanomechanical measurements of a superconducting qubit *Nature* **459** 960–4
[13] Arcizet O, Jacques V, Siria A, Poncharal P, Vincent P and Seidelin S 2011 A single nitrogen-vacancy defect coupled to a nanomechanical oscillator *Nature Phys.* **7** 879–83
[14] Kolkowitz S, Bleszynski Jayich A C, Unterreithmeier Q, Bennett S D, Rabl P, Harris J G E and Lukin M D 2012 Coherent sensing of a mechanical resonator with a single-spin qubit *Science* **355** 1603–6
[15] Fiore V, Yang Y, Kuzyk M C, Barbour R, Tian L and Wang H 2011 Storing optical information as a mechanical excitation in a silica optomechanical resonator *Phys. Rev. Lett.* **107** 133601
[16] Verhagen E, Deléglise S, Weis S, Schliesser A and Kippenberg T J 2012 Quantum-coherent coupling of a mechanical oscillator to an optical cavity mode *Nature* **482** 63–7
[17] Armour A D, Blencowe M P and Schwab K C 2002 Entanglement and decoherence of a micromechanical resonator via coupling to a Cooper-pair box *Phys. Rev. Lett.* **88** 148301
[18] Marshall W, Simon C, Penrose R and Bouwmeester D 2003 Towards quantum superpositions of a mirror *Phys. Rev. Lett.* **91** 130401
[19] Romero-Isart O, Pflanzer A C, Blaser F, Kaltenbaek R, Kiesel N, Aspelmeyer M and Cirac J I 2011 Large quantum superpositions and interference of massive nanometer-sized objects *Phys. Rev. Lett.* **107** 020405
[20] Pikovski I, Vanner M R, Aspelmeyer M, Kim M S and Brukner C 2012 Probing Planck-scale physics with quantum optics *Nature Phys.* **8** 393–7
[21] Weis S, Rivière R, Deléglise S, Gavartin E, Arcizet O, Schliesser A and Kippenberg T J 2010 Optomechanically induced transparency *Science* **330** 1520–3
[22] Safavi-Naeini A H, Mayer Alegre T P, Chan J, Eichenfield M, Winger M, Lin Q, Hill J T, Chang D E and Painter O 2011 Electromagnetically induced transparency and slow light with optomechanics *Nature* **472** 69–73
[23] Rabl P, Kolkowitz S J, Koppens F H L, Harris J G E, Zoller P and Lukin M D 2010 A quantum spin transducer based on nanoelectromechanical resonator arrays *Nature Phys.* **6** 602–8
[24] Stannigel K, Rabl P, Sørensen A S, Zoller P and Lukin M D 2010 Optomechanical transducers for long-distance quantum communication *Phys. Rev. Lett.* **105** 220501
[25] Safavi-Naeini A H and Painter O 2011 Proposal for an optomechanical traveling wave phonon–photon translator *New J. Phys.* **13** 013017
[26] Cirac J I and Zoller P 1995 Quantum computations with cold trapped ions *Phys. Rev. Lett.* **74** 4091–4
[27] Eisert J, Plenio M B, Bose S and Hartley J 2004 Towards quantum entanglement in nanoelectromechanical devices *Phys. Rev. Lett.* **93** 190402

[28] Schmidt M, Ludwig M and Marquardt F 2012 Optomechanical circuits for nanomechanical continuous variable quantum state processing arXiv:1202.3659 [cond-mat.mes-hall]
[29] Cirac J I, Zoller P, Kimble H J and Mabuchi H 1997 Quantum state transfer and entanglement distribution among distant nodes in a quantum network *Phys. Rev. Lett.* **78** 3221–4
[30] Kimble H J 2008 The quantum internet *Nature* **453** 1023–30
[31] Ritter S, Nolleke C, Hahn C, Reiserer A, Neuzner A, Uphoff M, Mucke M, Figueroa E, Bochmann J and Rempe G 2012 An elementary quantum network of single atoms in optical cavities *Nature* **484** 195–200
[32] Olsson R H III and El-Kady I 2009 Microfabricated phononic crystal devices and applications *Meas. Sci. Technol.* **20** 012002
[33] Safavi-Naeini A H and Painter O 2010 Design of optomechanical cavities and waveguides on a simultaneous bandgap phononic–photonic crystal slab *Opt. Express* **18** 14926–43
[34] Lüthi B 2005 *Physical Acoustics in the Solid State* (*Springer Series in Solid State Sciences*) (Berlin: Springer)
[35] Manipatruni S, Robinson J T and Lipson M 2009 Optical nonreciprocity in optomechanical structures *Phys. Rev. Lett.* **102** 213903
[36] Hafezi M and Rabl P 2012 Optomechanically induced non-reciprocity in microring resonators *Opt. Express* **20** 7672–84
[37] Buks E and Roukes M L 2002 Electrically tunable collective response in a coupled micromechanical array *J. Microelectromech. Syst.* **11** 802–7
[38] Gardiner C W and Zoller P 2004 *Quantum Noise* (Berlin: Springer)
[39] Marquardt F, Chen J P, Clerk A A and Girvin S M 2007 Quantum theory of cavity-assisted sideband cooling of mechanical motion *Phys. Rev. Lett.* **99** 093902
[40] Wilson-Rae I, Nooshi N, Zwerger W and Kippenberg T J 2007 Theory of ground state cooling of a mechanical oscillator using dynamical backaction *Phys. Rev. Lett.* **99** 093901
[41] Law C K 1995 Interaction between a moving mirror and radiation pressure: a Hamiltonian formulation *Phys. Rev.* A **51** 2537–41
[42] Kippenberg T J and Vahala K J 2007 Cavity opto-mechanics *Opt. Express* **15** 17172–205
[43] Stannigel K, Rabl P, Sørensen A S, Lukin M D and Zoller P 2011 Optomechanical transducers for quantum-information processing *Phys. Rev.* A **84** 042341
[44] Koch J, Houck A A, Le Hur K and Girvin S M 2010 Time-reversal-symmetry breaking in circuit-QED-based photon lattices *Phys. Rev.* A **82** 043811
[45] Nunnenkamp A, Koch J and Girvin S M 2011 Synthetic gauge fields and homodyne transmission in Jaynes–Cummings lattices *New J. Phys.* **13** 095008
[46] Karabalin R B, Cross M C and Roukes M L 2009 Nonlinear dynamics and chaos in two coupled nanomechanical resonators *Phys. Rev.* B **79** 165309
[47] Jelezko F and Wrachtrup J 2006 Single defect centres in diamond: a review *Phys. Status Solidi* a **203** 3207
[48] Tyryshkin A M *et al* 2012 Electron spin coherence exceeding seconds in high-purity silicon *Nature Mater.* **11** 143
[49] Mamin H J, Poggio M, Degen C L and Rugar D 2007 Nuclear magnetic resonance imaging with 90-nm resolution *Nature Nanotechnol.* **2** 301–6
[50] Rabl P, Cappellaro P, Gurudev Dutt M V, Jiang L, Maze J R and Lukin M D 2009 Strong magnetic coupling between an electronic spin qubit and a mechanical resonator *Phys. Rev.* B **79** 041302
[51] Palyi A, Struck P R, Rudner M, Flensberg K and Burkard G 2012 Spin–orbit induced strong coupling of a single spin to a nanomechanical resonator *Phys. Rev. Lett.* **108** 206811
[52] Ohm C, Stampfer C, Splettstoesser J and Wegewijs M R 2012 Readout of carbon nanotube vibrations based on spin–phonon coupling *Appl. Phys. Lett.* **100** 143103
[53] Etaki S, Poot M, Mahboob I, Onomitsu K, Yamaguchi H and van der Zant H S J 2008 Motion detection of a micromechanical resonator embedded in a d.c. squid *Nature Phys.* **4** 785
[54] Martin I, Shnirman A, Tian L and Zoller P 2004 Ground-state cooling of mechanical resonators *Phys. Rev.* B **69** 125339

[55] Zhou X and Mizel A 2006 Nonlinear coupling of nano mechanical resonators to Josephson quantum circuits *Phys. Rev. Lett.* **97** 267201
[56] Xue F, Wang Y D, Sun C P, Okamoto H, Yamaguchi H and Semba K 2007 Controllable coupling between flux qubit and nanomechanical resonator by magnetic field *New J. Phys.* **9** 35
[57] Jaehne K, Hammerer K and Wallquist M 2008 Ground-state cooling of a nanomechanical resonator via a Cooper-pair box qubit *New J. Phys.* **10** 095019
[58] Rabl P, Shnirman A and Zoller P 2004 Generation of squeezed states of nanomechanical resonators by reservoir engineering *Phys. Rev.* B **70** 205304
[59] Wilson-Rae I, Zoller P and Imamoğlu A 2004 Laser cooling of a nanomechanical resonator mode to its quantum ground state *Phys. Rev. Lett.* **92** 075507
[60] Soykal Ö O, Ruskov R and Tahan C 2011 Sound-based analogue of cavity quantum electrodynamics in silicon *Phys. Rev. Lett.* **107** 235502
[61] Maze J R, Gali A, Togan E, Chu Y, Trifonov A, Kaxiras E and Lukin M D 2011 Properties of nitrogen-vacancy centers in diamond: the group theoretic approach *New J. Phys.* **13** 025025
[62] Kielpinski D, Monroe C and Wineland D J 2002 Architecture for a large-scale ion-trap quantum computer *Nature* **417** 709
[63] Taylor J M, Engel H A, Dur W, Yacoby A, Marcus C M, Zoller P and Lukin M D 2005 Fault-tolerant architecture for quantum computation using electrically controlled semiconductor spins *Nature Phys.* **1** 177